

ICE NUCLEATION ON UNCOATED AND COATED
ATMOSPHERIC MINERAL DUST PARTICLES

by

MICHAEL LOGAN EASTWOOD

B. Sc., The University of British Columbia, 2002

A THESIS SUBMITTED IN PARTIAL FULFILLMENT OF
THE REQUIREMENTS FOR THE DEGREE OF

MASTER OF SCIENCE

in

THE FACULTY OF GRADUATE STUDIES

(Chemistry)

UNIVERSITY OF BRITISH COLUMBIA

(Vancouver)

August 2008

© Michael Logan Eastwood, 2008

ABSTRACT

An optical microscope coupled to a flow cell was used to investigate ice nucleation on five atmospherically relevant mineral dusts at temperatures ranging from 233 to 247 K. Kaolinite and muscovite particles were found to be efficient ice nuclei in the deposition mode, requiring relative humidities with respect to ice (RH_i) below 112% in order to initiate ice crystal formation. Quartz and calcite particles, by contrast, were poor ice nuclei, requiring relative humidities close to water saturation before ice crystals would form. Montmorillonite particles were efficient ice nuclei at temperatures below 241 K, but poor ice nuclei at higher temperatures. In several cases, there was a lack of quantitative agreement between these data and previously published work. This can be explained by several factors including mineral source, particle size, observation time and surface area available for nucleation.

Heterogeneous nucleation rates (J_{het}) were calculated from the onset data. J_{het} values ranged from 60 to 1100 $\text{cm}^{-2}\text{s}^{-1}$ for the five minerals studied. These values were then used to calculate contact angles (θ) for each mineral according to classical nucleation theory. The contact angles measured for kaolinite and muscovite ranged from 6 to 12°; for quartz and calcite the contact angles were much higher, ranging from 25 to 27°. The contact angles measured for montmorillonite were less than 15° at temperatures below 241 K, and above 20° at higher temperatures. The reported J_{het} and θ values may allow for a more direct comparison between laboratory studies and can be used when modeling ice cloud formation in the atmosphere.

The roles of H_2SO_4 and $(\text{NH}_4)_2\text{SO}_4$ coatings on the ice nucleating properties of kaolinite were also investigated. Onset data was collected for H_2SO_4 coated and $(\text{NH}_4)_2\text{SO}_4$ coated kaolinite particles at temperatures ranging from 233 to 247 K. In contrast to uncoated kaolinite particles, which were effective ice nuclei, H_2SO_4 coated particles were found to be poor ice nuclei, requiring relative humidities close to water saturation before nucleating ice at all temperatures studied. $(\text{NH}_4)_2\text{SO}_4$ coated particles were poor ice nuclei at 245 K, but effective ice nuclei at 236 K.

TABLE OF CONTENTS

ABSTRACT.....	ii
TABLE OF CONTENTS.....	iii
LIST OF TABLES.....	v
LIST OF FIGURES.....	vi
ACKNOWLEDGEMENTS.....	viii
1. Introduction.....	1
1.1 Aerosols.....	1
1.1.1 Aerosol impacts on climate.....	3
1.1.2 Aerosols as atmospheric ice nuclei.....	7
1.2 Mineral Dust.....	8
1.3 The Troposphere.....	10
1.4 Motivation for Research.....	12
1.5 Thesis Overview.....	13
2. Ice nucleation on mineral dust particles: onset conditions, nucleation rates and contact angles.....	14
2.1 Introduction.....	14
2.2 Experimental.....	16
2.2.1 Overview.....	16
2.2.2 Slide preparation.....	17
2.2.3 Sample preparation.....	17
2.2.4 Flow cell.....	19
2.2.5 Humidity control.....	20
2.2.6 Temperature calibration.....	23
2.2.7 Experimental procedure.....	26
2.3 Results and Discussion.....	28
2.3.1 Onset conditions.....	28

2.3.2 Heterogeneous nucleation rates	35
2.3.3 Classical nucleation theory	36
3. The effects of sulphuric acid and ammonium sulphate coatings	
on the ice nucleating properties of kaolinite	41
3.1 Introduction	41
3.2 Experimental	42
3.2.1 Overview	42
3.2.2 Sample preparation	43
3.2.3 Coated particle characterization	45
3.3 Results and Discussion	46
3.3.1 Uncoated kaolinite particles	46
3.3.2 H ₂ SO ₄ coated kaolinite particles	48
3.3.3 (NH ₄) ₂ SO ₄ coated kaolinite particles	52
4. Concluding remarks	55
4.1 Uncoated mineral dust	55
4.2 Coated mineral dust	56
4.3 Suggestions for future work	57
REFERENCES	58

LIST OF TABLES

Table 1.1: Source strengths of various aerosol species [adapted from <i>Forster et al.</i> , 2007]	2
Table 1.2: Common minerals present as atmospheric aerosols and their chemical formulae [<i>Berry et al.</i> , 1983; <i>Anthony et al.</i> , 1995]	8
Table 1.3: Mineralogy of Saharan dust collected at Sal Island (in the Cape Verde Islands), Barbados, and Miami, FL, after three large Saharan dust outbreaks. Percentages shown are averages of the three outbreaks (assuming 100% crystalline material) [<i>Glaccum and Prospero</i> , 1980]	9
Table 2.1: Chemical formulae of minerals studied [<i>Anthony et al.</i> , 1995]	18
Table 2.2: Summary of experimental conditions for previously published results	31
Table 2.3: J values and contact angles for all five minerals studied.	39

LIST OF FIGURES

Figure 1.1: Global mean RFs from selected agents and mechanisms, including levels of scientific understanding [adapted from <i>Forster et al.</i> , 2007].....	4
Figure 1.2: Schematic diagram of two aerosol indirect effects. The cloud on the left is representative of a normal atmospheric aerosol concentration, while the one on the right reflects an elevated concentration [adapted from <i>Forster et al.</i> , 2007].....	6
Figure 1.3: Heterogeneous modes of ice nucleation	7
Figure 1.4: Mean temperature profile of the Earth's atmosphere as a function of altitude [adapted from <i>Ahrens</i> , 1994].....	11
Figure 2.1: Schematic of the flow-cell used for these studies.....	16
Figure 2.2 Variation of $p_{liq} - p_{ice}$ as a function of temperature. The shaded region highlights the temperature range studied in these experiments	21
Figure 2.3: Ice crystal area and temperature as a function of time for a typical calibration experiment. By averaging the three highlighted results, the offset between hygrometer and the RTD at this temperature was determined to be $0.43 \pm 0.19^{\circ}\text{C}$	24
Figure 2.4: Calibration curve used to correct for the temperature difference between the RTD in the aluminum stage and the surface of the slide in the flow cell.....	25
Figure 2.5: Experimental trajectories used in these studies. Each trajectory is labelled with its corresponding frost point.....	26

Figure 2.6: Optical microscope images (100×) of kaolinite particles before (left) and after (right) ice nucleation.....	27
Figure 2.7: Onset conditions for all minerals studied.....	29
Figure 2.8: Summary of ice nucleation results for kaolinite	32
Figure 2.9: Summary of ice nucleation results for montmorillonite	34
Figure 2.10: Contact angle as a function of temperature for each mineral studied.....	40
Figure 3.1: Image of H ₂ SO ₄ -coated kaolinite particles prior to an ice nucleation experiment, collected using an optical microscope with a 10× objective....	44
Figure 3.2: (A) Image of two selected kaolinite particles coated with H ₂ SO ₄ at RH _w < 1%. (B) Image of the same two kaolinite particles coated with H ₂ SO ₄ at RH _w = 95%.....	46
Figure 3.3: Onset RH _i as a function of surface area for uncoated and coated kaolinite particles at 244 K	47
Figure 3.4: Summary of ice nucleation results for coated and uncoated kaolinite particles	48
Figure 3.5: Experimental trajectories and lines of constant droplet composition (in wt% H ₂ SO ₄).....	49
Figure 3.6: The crystal structure of kaolinite. Red = oxygen (O ²⁻), grey = aluminum (Al ³⁺), blue = silicon (Si ⁴⁺), yellow = hydrogen (H ⁺). Dotted lines represent hydrogen bonds holding two alumina-silicate sheets together.....	51
Figure 3.7: Schematic of the possible phase behaviour of an (NH ₄) ₂ SO ₄ coating during a typical freezing experiment	54

ACKNOWLEDGEMENTS

First and foremost, I would like to express my deep gratitude to Dr. Allan Bertram for giving me the opportunity to work in his lab as a graduate student for the past two and a half years. His advice was invaluable, his patience was always appreciated and his guidance is largely what made my research career at UBC so rewarding. Allan, thank you for all your support!

To my friends and colleagues from the Bertram group, both past and present, I extend my sincere thanks. To Dr. Ben J. Murray, for his thoughtful mentoring and tremendous assistance in getting my experimental work started so early. To Dr. Daniel A. Knopf, for his rigorous questioning (especially during talks) that kept me on my toes. To Dr. Matthew T. Parsons, for being a good friend who was always willing to share a laugh (or an enormous platter of barbequed meat). To Michael Wheeler, Sarah Hanna, Emily Simpson, Simone Gross, Lori Anthony, Dr. Sébastien Cremel and Dr. Pedro Campuzano-Jost, for being such friendly and helpful colleagues.

I would also like to express my appreciation to all the staff members from the Mechanical Shop, the Electronics Shop and the Glassblowing Shop for their assistance in various aspects of this project.

Finally, I would like to thank my family and friends for being so supportive during my return to UBC for a Master's degree. Especially during my final year when I was balancing a teaching job and research responsibilities, it was very helpful to receive encouragement from the people closest to me.

1. Introduction

1.1 Aerosols

Aerosols are suspensions of solid, liquid, or mixed solid-liquid particles in a gas [Seinfeld and Pandis, 1998]. Aerosols are ubiquitous in the atmosphere, present in concentrations from 10^2 to 10^6 cm^{-3} [Finlayson-Pitts and Pitts, 2000]. Aerosol particles have sizes ranging from clusters of a few molecules to $100\ \mu\text{m}$ and larger [Pruppacher and Klett, 1997], but those with diameters ranging from 0.002 – $10\ \mu\text{m}$ play the most significant role in terms of atmospheric chemistry and physics [Finlayson-Pitts and Pitts, 2000].

Aerosol particles have both natural and anthropogenic sources, with approximately 90% of emissions coming from natural sources [Andreae, 1995]. Atmospheric aerosols can be emitted directly as particles (primary aerosols) or formed in the atmosphere by gas-to-particle conversion processes (secondary aerosols) [Seinfeld and Pandis, 1998]. Table 1.1 provides the source strengths of various natural and anthropogenic species. Soil dust, sea salt and oceanic sulphate represent the largest fraction of the total natural aerosol abundance, while industrial dust and sulphates are the major components of aerosols produced by anthropogenic activities [d'Almeida et al., 1991; Andreae, 1995]. In the atmosphere, these particles have impacts in areas ranging from human health and visibility to atmospheric chemistry and climate.

Table 1.1: Source strengths of various aerosol species
[adapted from *d'Almeida et al.*, 1991; *Andreae*, 1995].

Source	Emission, Tg yr ⁻¹	Column burden, mg m ⁻²
<u>Natural</u>		
<i>Primary</i>		
Soil dust	1500	32.2
Sea-salt	1300	7.0
Volcanic dust	33	0.7
Biological debris	50	1.1
<i>Secondary</i>		
Sulphates	102	2.7
Organic matter	55	2.1
Nitrates	22	0.5
Total Natural	3060	46
<u>Anthropogenic</u>		
<i>Primary</i>		
Industrial dust	100	2.1
Black carbon	20	0.6
<i>Secondary</i>		
Sulphates	140	3.8
Biomass burning	80	3.4
Nitrates	36	0.8
Organic matter	10	0.4
Total Anthropogenic	390	11.1
TOTAL	3450	57
<i>Anthropogenic fraction</i>	11%	19%

1.1.1 Aerosol impacts on climate

In its Fourth Assessment Report, the Intergovernmental Panel on Climate Change (IPCC) stated that “it is *extremely likely*¹ that humans have exerted a substantial warming influence on climate” [Forster *et al.*, 2007]. *Radiative forcing* (RF) is a concept used to quantitatively compare the strengths of various human and natural agents in causing climate change, and is defined as “a change (usually expressed in Wm^{-2}) in the average net radiation at the tropopause due to a particular perturbation of interest” [Forster *et al.*, 2007]. Figure 1.1 illustrates the current best estimates for the RFs of a number of climate system components from 1750 to 2005.

There are two major reasons for researching the potential climate impacts of atmospheric aerosols. First, despite recent improvements in atmospheric models to represent all aerosol components of significance, the Fourth Assessment Report lists the level of scientific understanding for the total aerosol RF as *low* to *medium-low*. Second, the estimated cooling effect due to aerosols (RF = -0.4 to -2.7 Wm^{-2}) is potentially as large as the estimated warming effect due to rising greenhouse gas concentrations (RF = $+2.4$ to $+2.9 \text{ Wm}^{-2}$) [Forster *et al.*, 2007]. Further study in this field will strengthen the scientific community’s understanding of the mechanisms by which aerosols contribute to climate change and decrease the relatively large uncertainties associated with the current best estimates for the total aerosol RF.

¹ The use of ‘*extremely likely*’ is an example of the calibrated language used in the IPCC’s Fourth Assessment Report; it represents a 95% confidence level or higher.

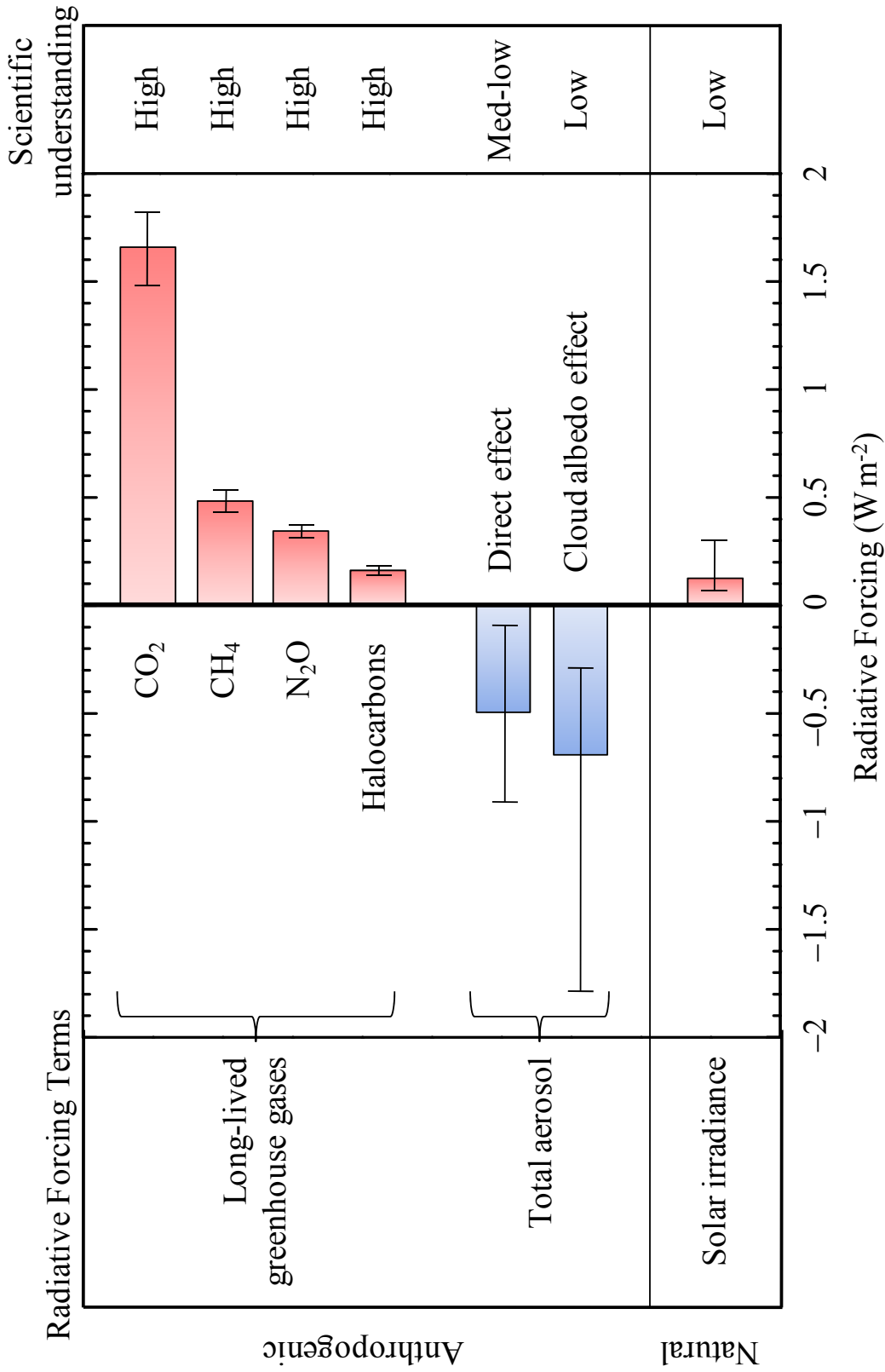


Figure 1.1: Global mean RFs from selected agents and mechanisms, including levels of scientific understanding. [adapted from Forster *et al.*, 2007]

The total aerosol RF can be considered as resulting from two different effects. The *direct aerosol effect* is defined as “the mechanism by which aerosols scatter and absorb shortwave and longwave radiation, thereby altering the radiative balance of the Earth-atmosphere system” [Forster *et al.*, 2007]. Of greater relevance to this thesis is the *indirect aerosol effect*, defined as “the mechanism by which aerosols modify the microphysical and hence the radiative properties, amount and lifetime of clouds” [Forster *et al.*, 2007]. The *aerosol indirect effect* can be further classified into:

- (1) the *cloud albedo effect*, which includes the effects of aerosols on the cloud droplet number concentration and hence cloud droplet size for fixed water content, [Twomey, 1974] and
- (2) the *cloud lifetime effect*, relating to changes in the water content, cloud height and lifetime of clouds caused by aerosols [Albrecht, 1989]

Aerosols contribute to these two effects primarily through their ability to act as cloud condensation nuclei (CCN) or ice nuclei (IN). An increase in aerosol concentration and hence an increase in the concentration of IN may lead to smaller cloud particles for a fixed water content (*cloud albedo effect*). A greater concentration of IN can also affect the precipitation efficiency, lifetime and optical depth of clouds (*cloud lifetime effect*). These processes are illustrated in Figure 1.2.

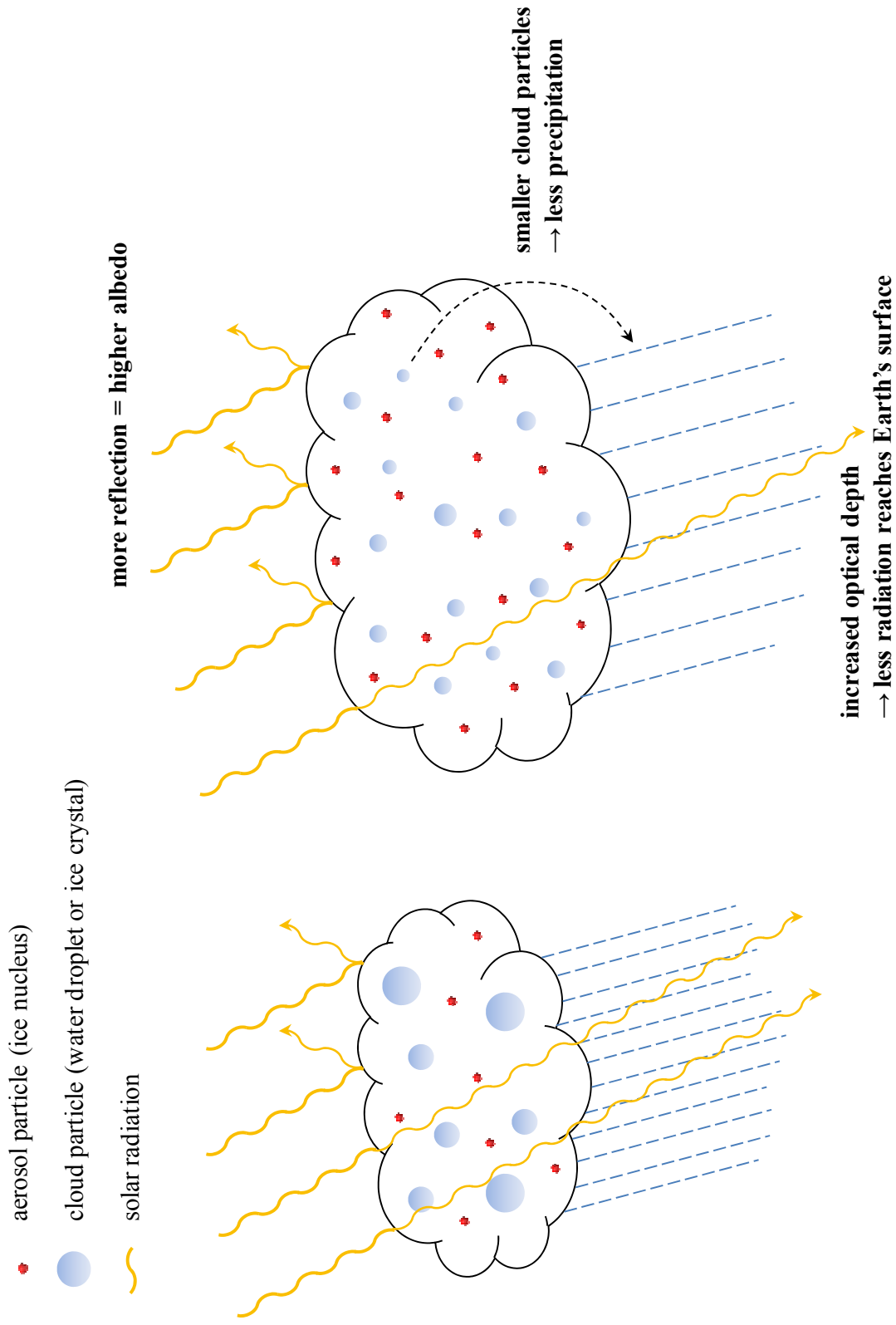


Figure 1.2: Schematic diagram of two aerosol indirect effects. The cloud on the left is representative of a normal atmospheric aerosol concentration, while the one on the right reflects an elevated concentration [adapted from *Forster et al., 2007*].

1.1.2 Aerosols as atmospheric ice nuclei

The formation of ice in the atmosphere occurs by one of two mechanisms: *homogeneous nucleation* or *heterogeneous nucleation*. Homogeneous ice nucleation is defined as the formation of ice from the gas or the liquid phase in the absence of foreign particles [Seinfeld and Pandis, 1998], and as such will not be discussed any further. Heterogeneous ice nucleation refers to the formation of an ice germ on a foreign substance such as an aerosol particle [Seinfeld and Pandis, 1998], and is thus of particular relevance to the studies presented hereafter.

Figure 1.3 summarizes the four modes of heterogeneous ice nucleation proposed by Vali [1985]. *Deposition nucleation* occurs when water vapour in an environment that is supersaturated with respect to ice and at temperatures below 0°C is adsorbed directly from the vapour phase onto the surface of an ice nucleus, where it transforms into ice. *Condensation freezing* occurs at relative humidities above water saturation, where an aerosol first acts as a cloud condensation nucleus to form a droplet, which then freezes. *Immersion freezing* refers to the process where an ice nucleus first becomes immersed in a water droplet, then freezes once its temperature has become sufficiently low. In *contact freezing*, ice nucleation is initiated when the ice nucleus comes in contact with a supercooled droplet.

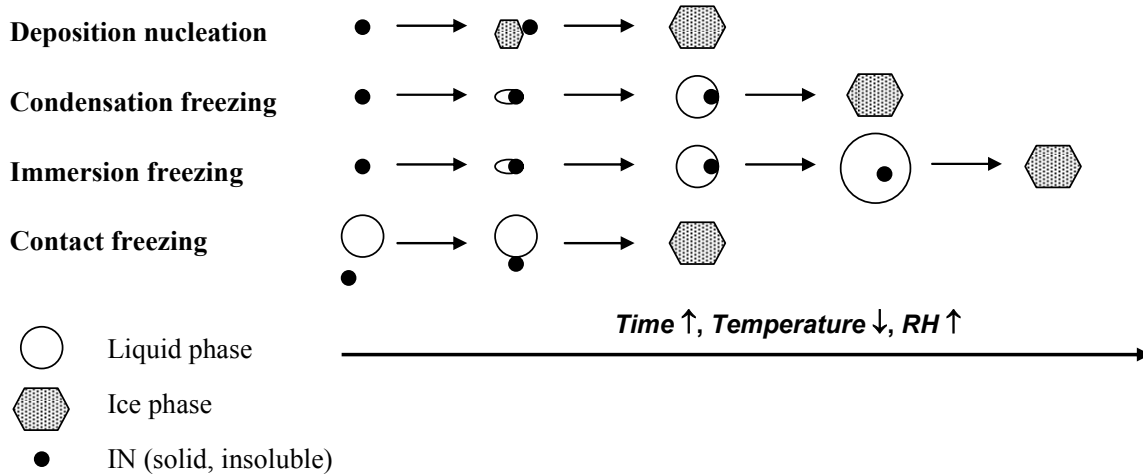


Figure 1.3: Heterogeneous modes of ice nucleation

1.2 Mineral Dust

Mineral dust particles are ubiquitous and abundant in the atmosphere, with estimates of global dust emissions to the atmosphere ranging from 500 to 5000 Mt/year [Peterson and Junge, 1971; d'Almeida, 1986; Schütz, 1987; Andreae, 1995; Duce, 1995; Tegen and Fung, 1995]. Mineral dust aerosols are soil particles that have been mobilized by strong wind currents and entrained into the atmosphere, and thus contain many of the same components as crustal rock [Usher *et al.*, 2003]. Table 1.2 lists some common minerals found in aerosolized dust and their chemical formulae.

Table 1.2: Common minerals present as atmospheric aerosols and their chemical formulae [Berry *et al.*, 1983; Anthony *et al.*, 1995].

Mineral	Formula
Calcite	CaCO_3
Chlorite	$\text{Y}_6\text{Z}_4\text{O}_{10}(\text{OH})_8$
Corundum	$\alpha\text{-Al}_2\text{O}_3$
Feldspar	XZ_4O_8
Gypsum	$\text{CaSO}_4 \cdot 2\text{H}_2\text{O}$
Hematite	$\alpha\text{-Fe}_2\text{O}_3$
Kaolinite	$\text{Al}_4\text{Si}_4\text{O}_{10}(\text{OH})_8$
Mica	$\text{XY}_{2-3}\text{Z}_4\text{O}_{10}(\text{O},\text{F},\text{OH})_2$
Montmorillonite	$(\text{Na},\text{Ca})(\text{Al},\text{Mg})_6(\text{Si}_4\text{O}_{10})_3(\text{OH})_6 \cdot n\text{H}_2\text{O}$
Palygorskite	$(\text{Al},\text{Mg})_2\text{Si}_4\text{O}_{10}(\text{OH}) \cdot 4\text{H}_2\text{O}$
Quartz	SiO_2

where $\text{X} = \text{Na}, \text{Ca}$ or K

$\text{Y} = \text{Al}, \text{Mg}$ or Fe

$\text{Z} = \text{Al}$ or Si

Table 1.3 lists the relative mineral composition of aerosol transported from North Africa and collected in Sal Island in the Cape Verde Islands, Barbados, and Miami [Glaccum and Prospero, 1980]. As dust is transported farther away from the source region, the larger, coarser particles typically composed of quartz and feldspars fall out of the atmosphere via gravitational settling. As a result, the overall composition tends to become enriched with the smaller, finer particles such as clays (e.g. kaolinite, montmorillonite) and micas (e.g. muscovite) [Usher *et al.*, 2003].

Table 1.3: Mineralogy of Saharan dust collected at Sal Island (in the Cape Verde Islands), Barbados, and Miami, FL, after three large Saharan dust outbreaks. Percentages shown are averages of the three outbreaks (assuming 100% crystalline material) [Glaccum and Prospero, 1980].

Mineral	Sal Island	Barbados	Miami
Mica	53.8%	64.3%	62.1%
Quartz	19.6%	13.8%	14.2%
Kaolinite	6.6%	8.3%	7.1%
Calcite	8.2%	3.9%	6.9%
Plagioclase [†]	5.4%	4.1%	4.5%
Chlorite	4.3%	4.1%	4.2%
Montmorillonite	≤ 5 %	≤ 5 %	≤ 5 %

[†] member of the feldspar mineral group

1.3 The Troposphere

The region of the atmosphere extending from the Earth's surface to the height where air ceases to become colder with height is called the *troposphere* [Finlayson-Pitts and Pitts, 2000]. Figure 1.4 illustrates the mean temperature of the Earth's atmosphere as a function of altitude and gives the height of the troposphere as approximately 11 km [Ahrens, 1994], but its height ranges from 8 to 18 km depending on the latitude and season [Wayne, 2000]. The troposphere is kept well stirred by rising and descending air currents, and contains all of the weather we are familiar with on Earth [Ahrens, 1994]. In order to maximize the atmospheric relevance of the research presented in this thesis, the experiments described herein were performed over a temperature range (233 to 247 K) that is relevant for the troposphere.

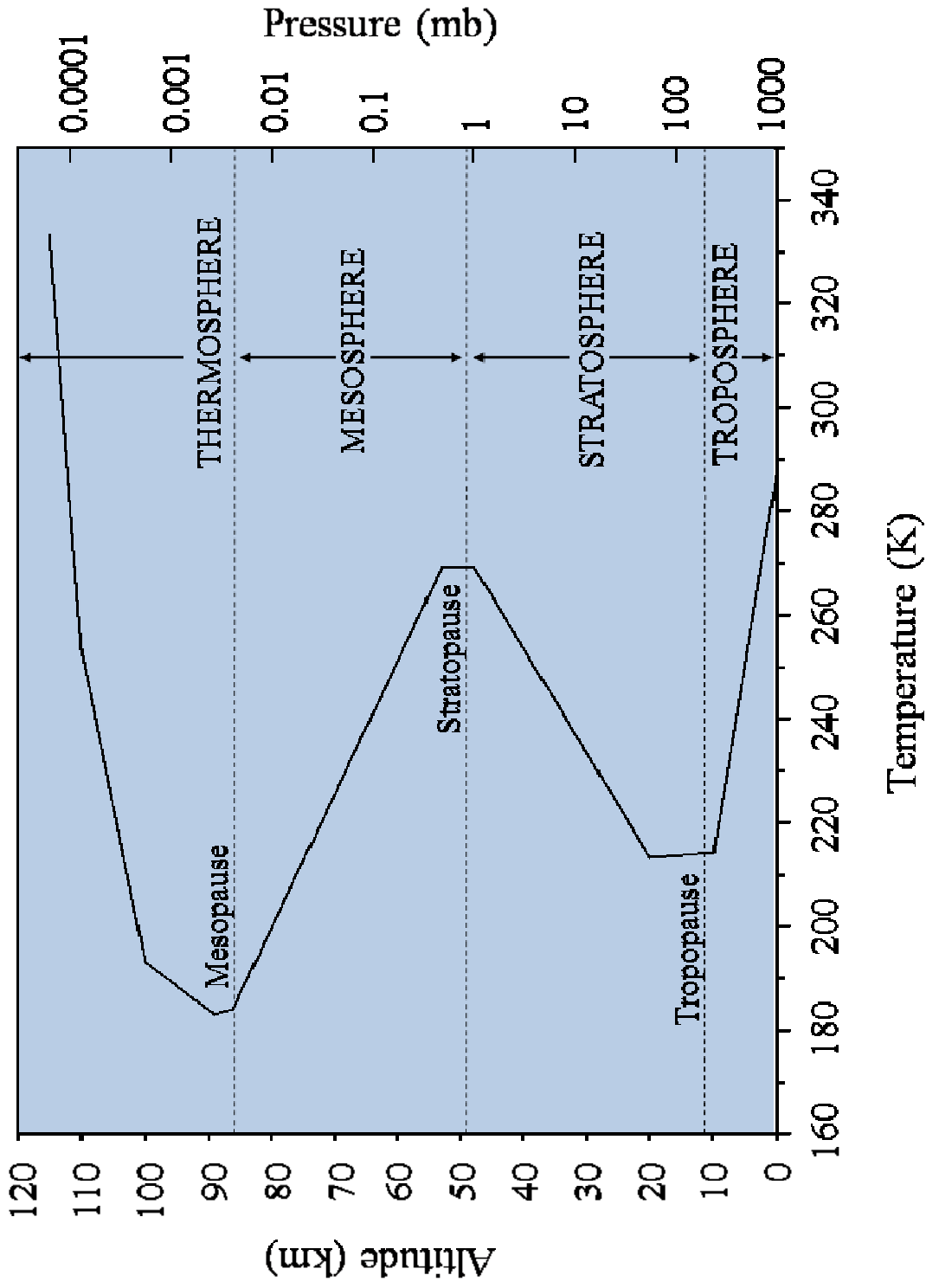


Figure 1.4: Mean temperature profile of the Earth's atmosphere as a function of altitude [adapted from Ahrens, 1994]

1.4 Motivation for Research

Particulate matter such as mineral dusts can have a number of effects in the atmosphere, but here the focus is on climate effects. Climate forcing by particulates is currently recognized as one of the greatest uncertainties in global circulation models, which are used to make predictions about climate change [Haywood and Boucher, 2000; Sokolik *et al.*, 2001]. Particulates can alter the chemical balance of the atmosphere, changing its thermodynamic and optical properties, which can result in climate forcing as the absorption and scattering of solar radiation is affected [Usher *et al.*, 2003]. The relative impact of atmospheric mineral dusts on climate forcing remains poorly quantified due to an incomplete understanding of the transport and removal processes, and the chemical and physical properties of the particles [Sokolik, 2001].

In its latest assessment report, the IPCC only considered the contribution of CCN to the RF resulting from the indirect aerosol effect. Although the IPCC acknowledges that IN such as mineral dust particles likely play a key role in cloud formation processes, understanding of this role was deemed insufficient [Forster *et al.*, 2007]. This lack of understanding, which in turn contributes to the large uncertainties associated with the estimated RF resulting from aerosol effects, is the key motivation for the research presented in this thesis.

1.5 Thesis Overview

This thesis is presented in four chapters. This chapter discussed relevant background information relating to aerosols, ice nuclei, mineral dust and the atmosphere. Chapter 2 focuses on the ice nucleating properties of uncoated mineral dusts. Onset relative humidities are reported, heterogeneous nucleation rates (J_{het}) are calculated, and then classical nucleation theory is employed to determine the contact angles (θ) between the critical ice nuclei and the mineral surfaces. Chapter 3 focuses on the effects of inorganic coatings (H_2SO_4 and $(\text{NH}_4)_2\text{SO}_4$) on the ice nucleating properties of kaolinite. Finally, a brief summary of the results and suggestions for future experiments are presented in Chapter 4.

2. Ice nucleation on mineral dust particles: onset conditions, nucleation rates and contact angles

2.1 Introduction

The scientific community's lack of data on ice nucleation processes is a major obstacle for the simulation of the complex interactions between aerosols and cold clouds. It has been shown in various investigations [Girard and Curry, 2001; Girard *et al.*, 2005; Avramov, 2006] that mixed-phase clouds often cannot be properly simulated with the existing parameterizations such as those of Fletcher [1962] and Meyers *et al.* [1992]. More physically-based parameterizations are needed to simulate heterogeneous nucleation in climate models.

Mineral dust particles are abundant in the atmosphere, and both laboratory [Pruppacher and Klett, 1997; Bailey and Hallett, 2002; DeMott, 2002; Zuberi, 2002; Hung *et al.*, 2003; Archuleta *et al.*, 2005; Mangold *et al.*, 2005; Möhler *et al.*, 2006; Field *et al.*, 2006; Knopf and Koop, 2006; Marcolli *et al.*, 2007; Zimmermann *et al.*, 2007] and field measurements [Sassen *et al.*, 2002; DeMott *et al.*, 2003a; DeMott *et al.*, 2003b; Sassen *et al.*, 2003; Toon, 2003; Cziczo *et al.*, 2004; Sassen, 2005; Twohy and Poellot, 2005; Kanji and Abbatt, 2006] have shown that mineral dust particles are effective ice nuclei. Laboratory data have shown that mineral dust particles can lower the supersaturations and temperatures required for ice formation compared to homogeneous nucleation. At the same time, field measurements have shown that mineral dust particles can have a significant impact on cloud formation, cloud properties and precipitation [Sassen *et al.*, 2002; DeMott *et al.*, 2003a; Sassen *et al.*, 2003; Sassen, 2005]. Measurements have also shown that the cores of ice crystals often contain mineral dust particles, suggesting that ice nucleation is often initiated by mineral dust aerosols in the atmosphere [Heintzenberg *et al.*, 1996; Cziczo *et al.*, 2004; Twohy and Poellot, 2005]. Furthermore, measurements have shown that mineral dust comprises a significant fraction of atmospheric ice nuclei. [Chen *et al.*, 1998; DeMott *et al.*, 2003b].

Although there have been numerous studies on the ice nucleating properties of mineral dust particles, more work is still needed for a complete understanding of the role

these particles play as atmospheric ice nuclei [Vali, 1996; Martin, 2000; Cantrell and Heymsfield, 2005]. Only a few of the most abundant types of minerals found in the atmosphere have been studied in detail. In addition, many of the previous studies only reported the onset conditions for ice nucleation; only a few considered nucleation rates (a key parameter for describing ice nucleation). Measurements of nucleation rates are needed in order to more accurately compare laboratory results and to extrapolate laboratory data to the atmosphere.

As pointed out by Vali [1996] in a review on ice nucleation, the origin of ice in lower tropospheric clouds is not resolved, and it remains a question of great importance and in need of new efforts. This chapter focuses on the ice nucleating properties of mineral dust particles at temperatures between 233 and 247 K, a temperature range relevant for the troposphere. To date, few measurements have been made at these particular temperatures.

Five commercial mineral dusts were selected for this study. Specifically, the ice nucleation properties of muscovite (a common mineral in the mica group), kaolinite, montmorillonite, quartz and calcite particles were investigated. These minerals were chosen since they are major components of aerosolized mineral dust found in the atmosphere. To illustrate this point, the mineralogy of Saharan dust collected in Sal Island, Barbados and Miami after three large Saharan dust outbreaks are shown in Table 1.3 on page 9 [Glaccum and Prospero, 1980]. The minerals chosen for this study represent over 90% of the total mass during these outbreaks. Montmorillonite composition was below the detection limit (5%) in the Saharan dust studies illustrated in Table 1.3, but several studies have cited montmorillonite as one of the dominant clay minerals present in African and Asian dusts [Schütz, 1989; Schütz, 1997; Prospero, 1999; Hanisch and Crowley, 2001].

This chapter is organised as follows: first, measurements of the onset conditions for ice nucleation on muscovite, kaolinite, montmorillonite, quartz and calcite are presented. Here, the onset conditions are defined as the relative humidity with respect to ice (RH_i) and temperature at which the first ice nucleation event was observed. Second, these data are compared with existing data in the literature. Third, heterogeneous ice nucleation rates (number of nucleation events per unit surface area of solid material per

unit time) are determined from the onset data for each mineral type. Fourth, the heterogeneous nucleation rates are parameterized using classical nucleation theory, and contact angles between the mineral surfaces and the critical ice nuclei are calculated.

2.2 Experimental

2.2.1 Overview

The apparatus used in this study consisted of an optical microscope coupled to a flow-cell (see Figure 2.1) in which the humidity and temperature could be accurately controlled. Mineral dust particles were deposited on the bottom surface of the flow cell and the relative humidity inside the cell was slowly increased. Ice crystal formation was observed with a reflected-light microscope (Zeiss Axiotech 100) equipped with a 10× objective lens. From these measurements, the onset conditions (temperature and relative humidity) for ice nucleation were determined.

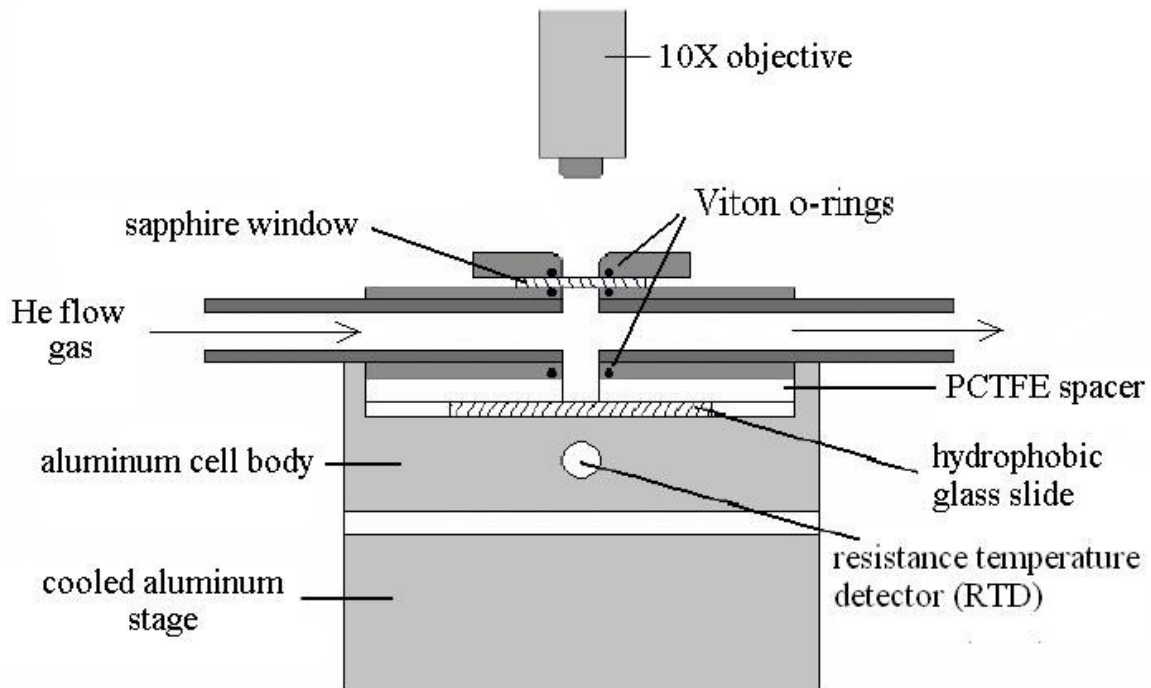


Figure 2.1: Schematic of the flow-cell used for these studies.

2.2.2 Slide preparation

The bottom surface of the flow cell was a glass cover slide that had been treated with dichlorodimethylsilane (DCDMS) to make a hydrophobic layer, which reduced the probability of ice nucleation directly on the surface. Each glass slide was first cleaned with a dry ice cleaning system (Sno Gun-II™, Va-Tran Systems) to remove any coarse impurities from the slide surface. The slides were then immersed in “piranha” solution (3:1 mixture by volume of concentrated sulphuric acid and 30% hydrogen peroxide) for approximately 10 minutes, then rinsed with high purity water (distilled water further purified with a Millipore Simplicity 185 system, 18.2 MΩ) and methanol (HPLC grade). The slides were then dried with a flow of high-purity N₂ (99.999%). Finally, each glass slide was treated with the dry ice cleaning system and rinsed with high purity water and methanol for a second time. After being dried with high-purity N₂ gas once again, the clean slide was placed in an airtight glass chamber. The final step involved adding 3 droplets of DCDMS solution (Fluka, 5% DCDMS in heptane) to the chamber, but not directly on the slides. Left overnight, the DCDMS coated the glass slides via vapour deposition.

2.2.3 Sample preparation

Five different types of mineral dust were studied in these experiments. Muscovite particles were generated by grinding muscovite flakes (1–10 mm in diameter, <1 mm in thickness, purchased from Alfa Aesar) with a mortar and pestle. Quartz particles were produced by grinding a sample of quartz tubing (purchased from United Silica) with a mortar and pestle. Kaolinite (purchased from Fluka), montmorillonite (purchased from Fluka) and calcite (purchased from Puratronic®, Alfa Aesar) particles were used as supplied. The chemical formulae of these minerals are listed in Table 2.1.

Table 2.1: Chemical formulae of minerals studied [Anthony *et al.*, 1995]

Mineral	Formula
Muscovite	$\text{KAl}_2(\text{Si}_3\text{Al})\text{O}_{10}(\text{OH},\text{F})_2$
Kaolinite	$\text{Al}_4\text{Si}_4\text{O}_{10}(\text{OH})_8$
Quartz	SiO_2
Calcite	CaCO_3
Montmorillonite	$(\text{Na},\text{Ca})(\text{Al},\text{Mg})_6(\text{Si}_4\text{O}_{10})_3(\text{OH})_6 \cdot n\text{H}_2\text{O}$

All samples were prepared and the flow cell constructed within a filtered air laminar flow hood. This greatly reduced the possibility of sample contamination by ambient atmospheric and laboratory particles. All mineral dust particles with the exception of calcite were deposited on the hydrophobic glass slide using the following technique: the dry dust particulates were placed in a glass vessel immersed in an ultrasonic bath. A flow of ultra-high purity N_2 was passed through the glass vessel, and vibrations from the ultrasonic bath caused the dust particles to be suspended in the flow of N_2 . This flow was then directed at the hydrophobic glass slide, and the dust particles were deposited on the slide by impaction. Calcite particles were not readily suspended by the vibrations from the ultrasonic bath, so these were deposited on the hydrophobic slide simply by sprinkling them directly on the slide using a small spatula. In all cases, dust particles deposited on the slide were less than $50 \mu\text{m}$ in diameter. The optical resolution limit of the microscope was $\sim 1 \mu\text{m}$. A typical sample held between 100 to 1000 individual particles, the majority of which were between 1 and $20 \mu\text{m}$ in diameter.

2.2.4 Flow cell

The flow cell, illustrated previously in Figure 2.1, was positioned on a cooling stage. The temperature of the cooling stage and hence the flow cell was regulated with a refrigerating circulator (Thermo Neslab ULT-95). The hydrophobic slide, which supported the particles, was positioned inside the aluminum cell body. An insulating spacer, made from polychloro-trifluoroethylene (PCTFE), was placed between the hydrophobic glass slide and the flow cell body. This ensured that the coldest component of the flow cell was the glass substrate (by ~ 10 K), thus preventing ice nucleation from occurring anywhere else in the cell. All seals within the cell were made with Viton O-rings with the exception of the seal between the glass slide and the PCTFE spacer, which was made with low vapour pressure chlorotrifluoroethylene grease (Series 28LT from Halocarbon Products). The grease ensured that no space remained between the glass slide and the PCTFE spacer, where ice could nucleate without being detected by the microscope.

The upper portion of the cell body and the inlet and outlet were made from stainless steel. A sapphire window (1 mm thick) was positioned at the top of the cell body, allowing optical access to the bottom surface of the cell. The reflected-light microscope was coupled to a high-resolution monochrome digital video camera (Sony, XCD-X700) which captured images of the particles deposited on the hydrophobic slide during the course of the experiments.

2.2.5 Humidity control

During the ice nucleation experiments, a flow of humidified helium gas was introduced to one side of the cell and exited on the other where its frost point was measured with a hygrometer (General Eastern 1311DR). Helium was chosen as the carrier gas because it diffuses to the particles on the slide more rapidly than nitrogen or argon.

From the frost point measurements, the saturation vapour pressure over ice (p_{ice}) in units of Pa was calculated using the parameterization of *Murphy and Koop* [2005], given by:

$$p_{ice} = \exp(9.550426 - 5723.265/T + 3.53068\ln(T) - 0.00728332T); \quad T > 110 \text{ K} \quad (2.1)$$

The saturation vapour pressure of supercooled water (p_{liq}) in units of Pa was calculated from the temperature using another parameterization proposed by *Murphy and Koop* [2005], given as follows:

$$\begin{aligned} \ln(p_{liq}) = & 54.842763 - 6763.22/T - 4.210\ln(T) + 0.000367T \\ & + \tanh\{0.0415(T - 218.8)\}(53.878 - 1331.22/T \\ & - 9.44523\ln(T) + 0.014025T) \end{aligned}$$

for $123 < T < 332 \text{ K}$ (2.2)

Figure 2.2 illustrates the difference between p_{liq} and p_{ice} as a function of temperature. For the temperature range used in these studies (233 to 247 K), the saturation vapour pressure over liquid water is 6 to 16 Pa greater than that over ice.

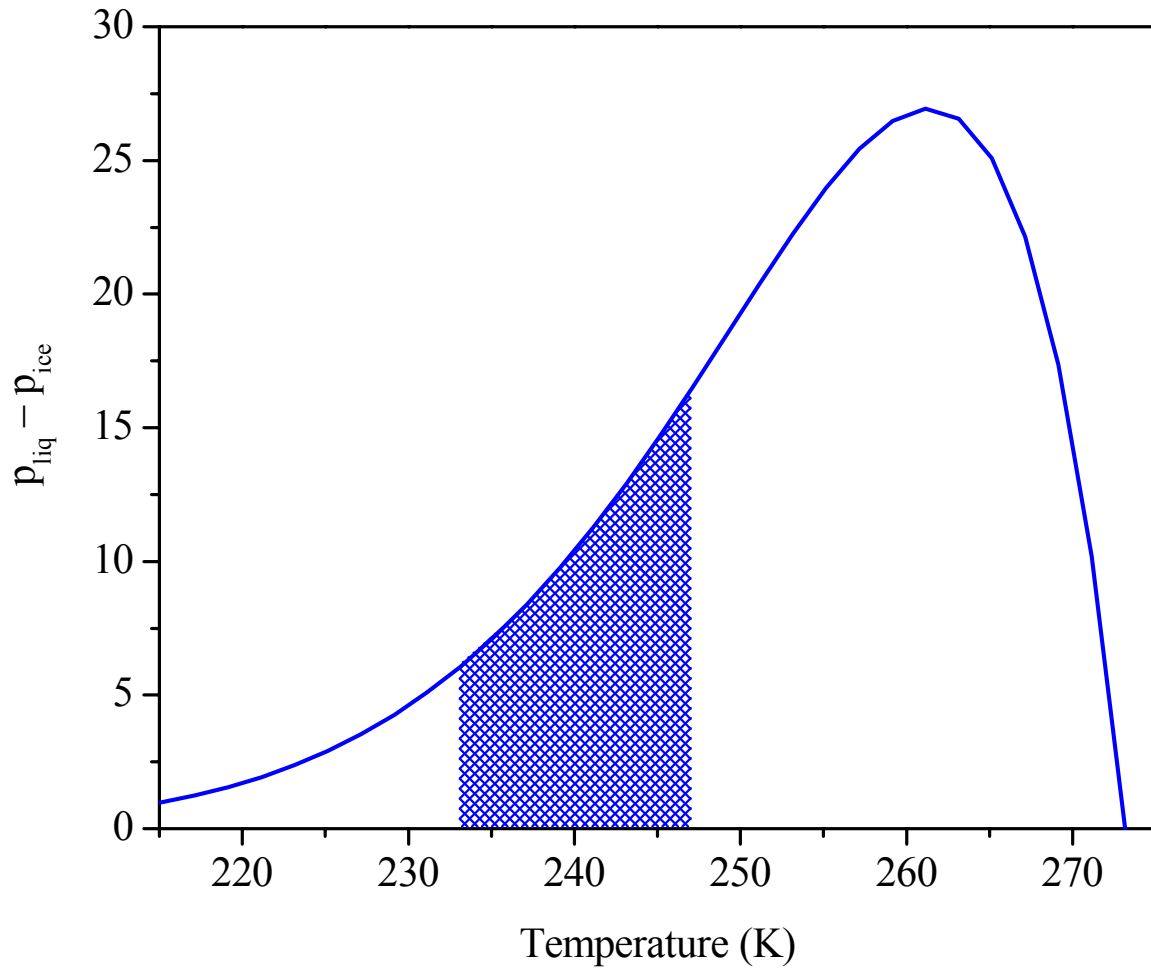


Figure 2.2: Variation of $p_{\text{liq}} - p_{\text{ice}}$ as a function of temperature. The shaded region highlights the temperature range studied in these experiments.

The relative humidity with respect to ice (RH_i) inside the flow cell was determined as follows:

$$RH_i = \frac{p_{ice}(T_{frost})}{p_{ice}(T_{cell})} \times 100\% \quad (2.3)$$

where $p_{ice}(T_{frost})$ is the vapour pressure of water inside the cell, calculated from Equation 2.1 using frost point (T_{frost}) measurements made by the hygrometer, and $p_{ice}(T_{cell})$ is the saturated vapour pressure (with respect to ice) inside the cell, also calculated from Equation 2.1, but at the temperature of the cell (T_{cell}).

The relative humidity with respect to water (RH_w) is determined as follows:

$$RH_w = \frac{p_{ice}(T_{frost})}{p_{liq}(T_{cell})} \times 100\% \quad (2.4)$$

where $p_{liq}(T_{cell})$ is the saturated vapour pressure (with respect to water) inside the cell, calculated from Equation 2.2 at the temperature of the cell.

The flow of humidified gas was generated by passing a flow of ultra-high purity He gas (99.999%) over a reservoir of ultra-pure water (distilled water further purified using a Millipore system). The humidity was set by altering the temperature of the water reservoir and diluting the humidified flow with a second flow of dry He. A continuous flow of between 1900 to 2100 $\text{cm}^3 \text{min}^{-1}$ (at 273.15 K and 1 atm) was maintained throughout the course of the ice nucleation experiments.

For purification, the He gas used in these experiments was first passed through a trap containing molecular sieve (1/16" pellets, Type T4A) at 77 K and then through a 0.02 μm filter (Anodisc 25).

2.2.6 Temperature calibration

In the experimental apparatus (illustrated previously in Figure 2.1), a Pt-100 resistance temperature detector (RTD) was located beneath the slide supporting the mineral dust particles. The temperature reported by the RTD was slightly lower than that of the dust particles being studied. Calibrations were performed to determine the offset between the temperature given by the RTD and the temperature of the particles by observing the change in size of ice crystals on the slide as the temperature was ramped up and down. The RTD was calibrated against the frost point within the cell, as done previously by *Middlebrook et al.* [1993] and *Parsons et al.* [2004]. The temperature at which the size of the ice crystals remained constant was determined. At this temperature, the ice crystals were in equilibrium with the water vapour inside the cell, whose frost point was precisely known. The temperature offset determined using this technique was used to correct experimentally measured temperatures obtained with the RTD.

The results from one calibration experiment performed at a frost point of 236.7 K are shown in Figure 2.3. The offset between the RTD and the hygrometer was determined to be 0.21°C at 246.7 K, 0.31°C at 241.7 K, and 0.43°C at 236.7 K. A calibration curve, illustrated in Figure 2.4, was generated from these data and used to correct the RTD reading in all experiments.

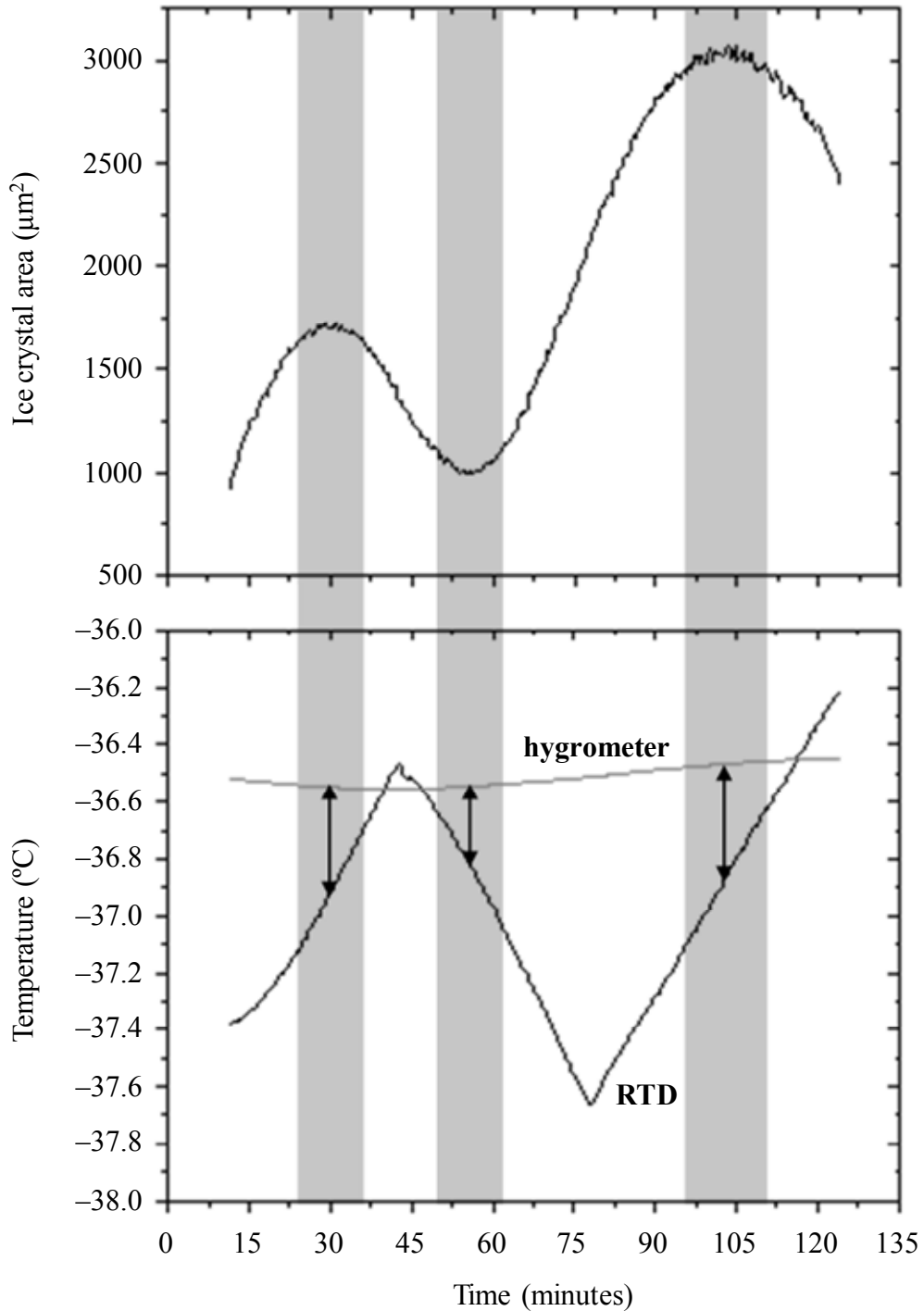


Figure 2.3: Ice crystal area and temperature as a function of time for a typical calibration experiment. By averaging the three highlighted results, the offset between hygrometer and the RTD at this temperature was determined to be $0.43 \pm 0.19^{\circ}\text{C}$.

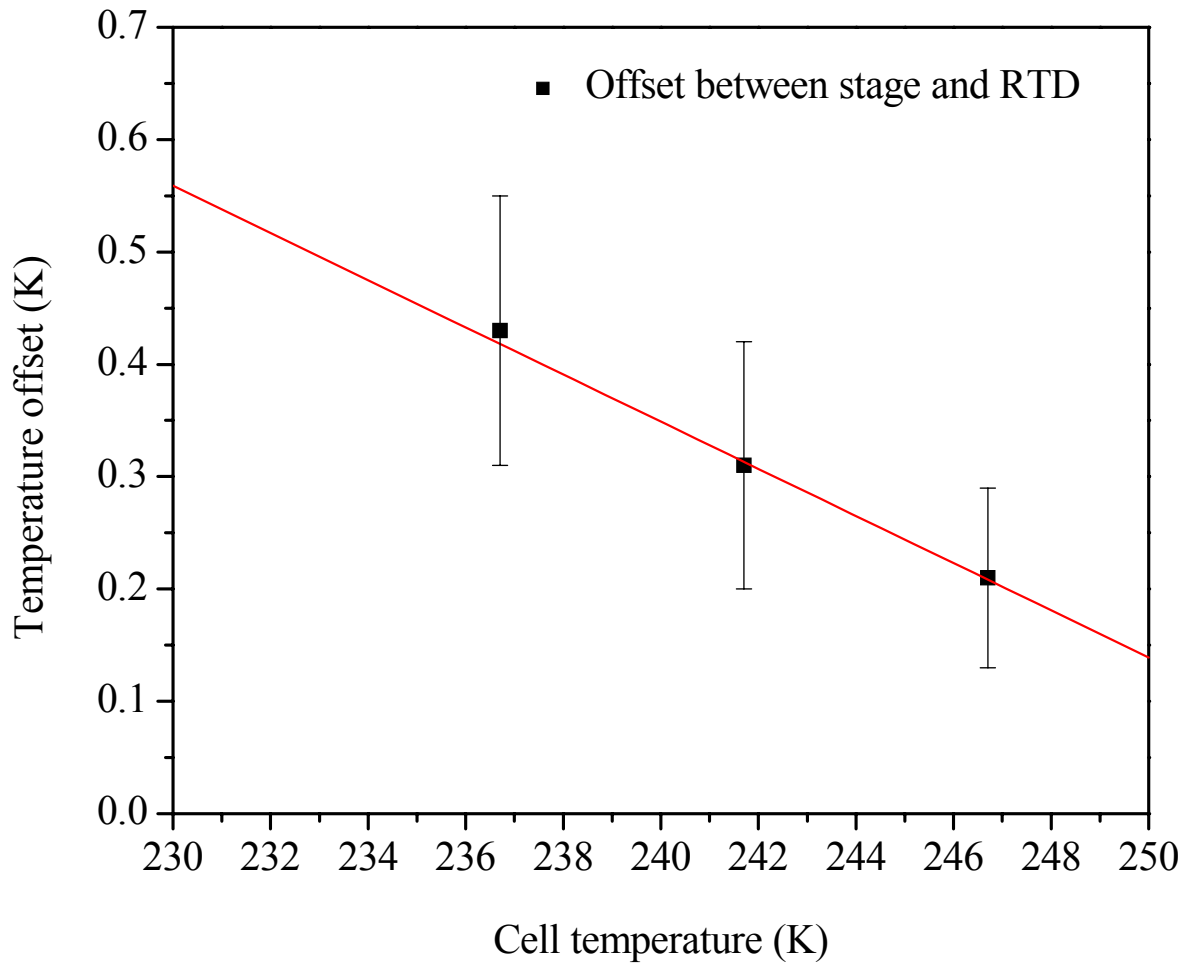


Figure 2.4: Calibration curve used to correct for the temperature difference between the RTD in the aluminum stage and the surface of the slide in the flow cell.

2.2.7 Experimental procedure

In each nucleation experiment, the RH_i in the flow cell was ramped from approximately 95% to water saturation (135–150%, depending on the temperature) by decreasing the temperature of the cell at approximately 0.08 K min^{-1} while maintaining a constant frost point inside the cell. During these experiments, the RH_i increased at an approximate rate of $1\% \text{ min}^{-1}$. Figure 2.5 illustrates the three experimental RH_i trajectories used in these studies, taken at frost points of 236.7, 241.7, and 246.7 K.

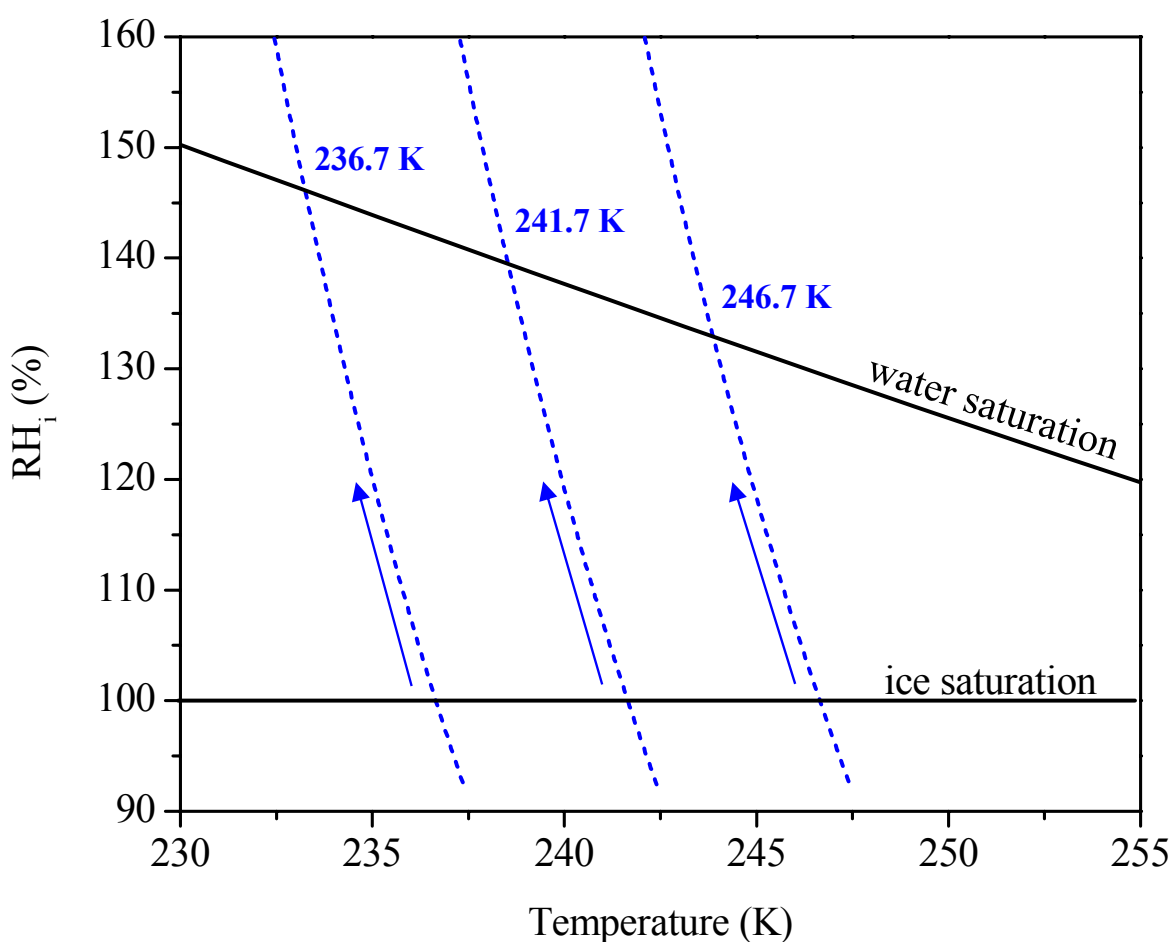


Figure 2.5: Experimental trajectories used in these studies. Each trajectory is labelled with its corresponding frost point.

Images of the dust particles were recorded digitally every 20 seconds (corresponding to a temperature decrease of ~ 0.027 K or an RH_i increase of $\sim 0.3\%$), while simultaneously recording p_{ice} and the cell temperature. From these images, the RH_i at which ice crystals first formed was determined (i.e. the onset of ice nucleation). Shown in Figure 2.6 are images of kaolinite particles recorded in a typical freezing experiment before and after ice nucleation, respectively. The formation of ice crystals is clearly discernable.

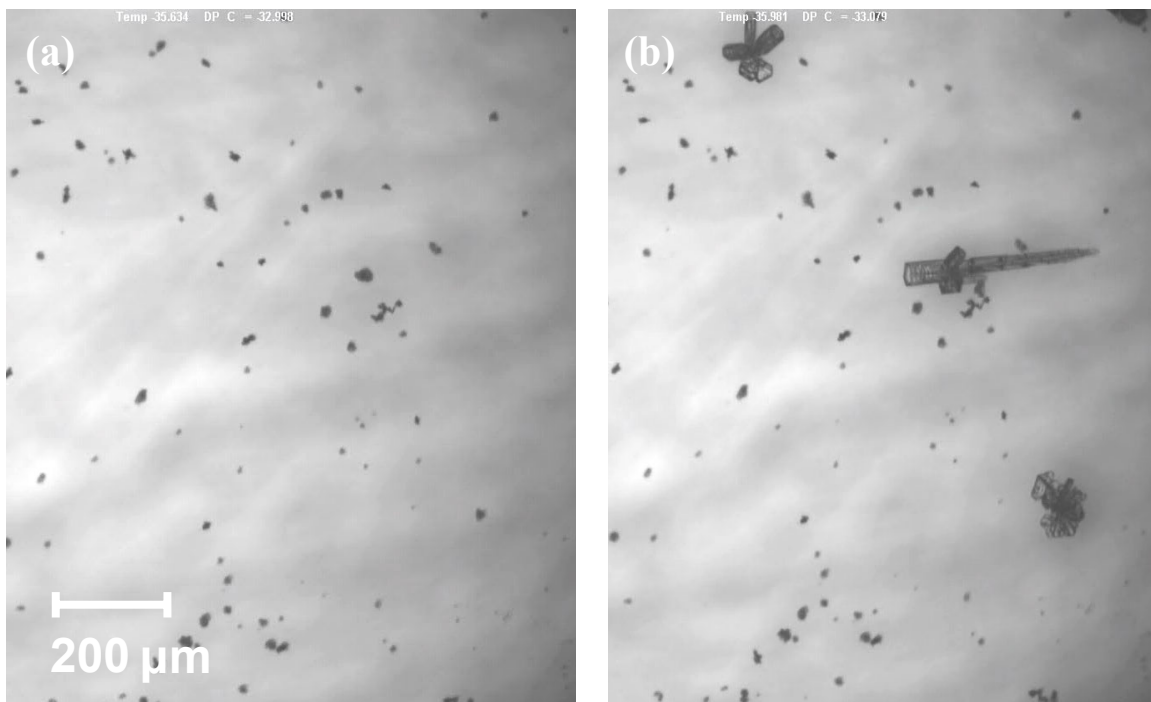


Figure 2.6: Optical microscope images (100 \times) of kaolinite particles before (left) and after (right) ice nucleation.

2.3 Results and Discussion

2.3.1 Onset conditions

Shown in Figure 2.7 are the onset conditions for all five minerals at each of the three temperatures studied. The error bars represent 95% confidence intervals based on at least six measurements per data point. Based on Figure 2.7, kaolinite and muscovite are effective ice nuclei at all temperatures studied, with onset RH_i values below 112%. Quartz and calcite were poor ice nuclei at all temperatures studied, requiring relative humidities close to water saturation before ice nucleation occurred. Montmorillonite was an effective ice nucleus at the two lowest temperatures studied (236.0 and 240.8 K), but a relatively poor ice nucleus at the highest temperature studied (244.6 K). Overall, the data show significant differences in the ice nucleating abilities of the five minerals studied over this temperature range.

The reason why some minerals are better ice nuclei than others is still relatively poorly understood. However, previous research suggests that it is likely a combination of the strengths of the chemical bonds at the mineral surface, the crystallographic match between the substrate and ice embryo, and the presence of active sites on the mineral surface, which can promote ice nucleation [Pruppacher and Klett, 1997]. For example, it has been speculated that kaolinite's ability to act as an ice nucleus may be due to the pseudo-hexagonal arrangement of the hydroxyl ($-OH$) groups at the kaolinite surface [Pruppacher and Klett, 1997]. These results provide further data that can be used to test these various theories.

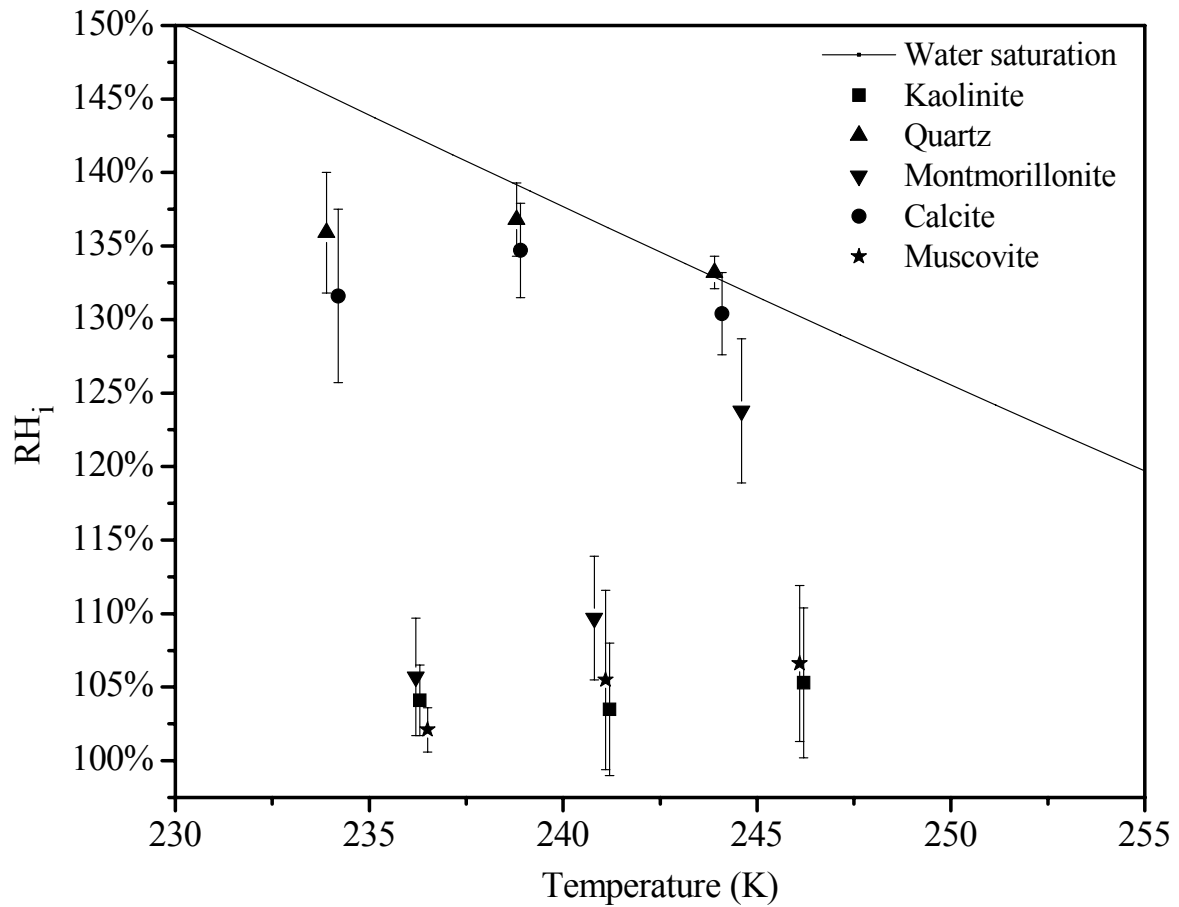


Figure 2.7: Onset conditions for all minerals studied

For all results where the onset conditions were below the water saturation line in Figure 2.7, the data correspond to deposition freezing, which occurs when water vapour adsorbs onto a solid surface and is then transformed into ice [Vali, 1996]. The data that overlap with the water saturation line in Figure 2.7, on the other hand, may have occurred by either deposition freezing or condensation freezing. Condensation freezing refers to the sequence of events whereby liquid water first condenses followed by freezing of the liquid [Vali, 1996]. In these experiments, there was no observation of liquid water droplet formation prior to ice, but the size of the water droplets may have been below the detection limit of the microscope, or else the water droplets only formed for a short amount of time and were not observed.

The mineral particles in these experiments are suspended on a hydrophobic glass substrate. Before further discussing the data, the possible effect of the hydrophobic glass substrate on the ice nucleation results must be addressed. First, in blank experiments (when no mineral dust was used) ice nucleation did not occur below liquid water saturation, and liquid water droplets always formed (and were clearly visible with the microscope) when liquid water supersaturation was reached [Dymarska *et al.*, 2006]. Occasionally, ice would form after the formation of liquid water droplets, but liquid water droplets were always observed first. This is very different from the results observed with mineral dust particles, where in many cases ice nucleation occurred below water saturation, and there was never any indication of the formation of liquid water droplets. Second, direct observations of the optical images confirmed that ice nucleation always occurred on a mineral particle, rather than a bare spot on the hydrophobic glass substrate. Third, tests were performed with two other types of supports to further ensure that the hydrophobic glass slide was not influencing the results. The ice nucleation experiments were repeated using bare glass slides that were cleaned as usual, but not coated with the hydrophobic DCDMS layer, resulting in a hydrophilic substrate. Also, experiments were performed using thin Teflon sheets as the bottom surface of the flow cell. Within the uncertainty of the measurements, the onset results were independent of the type of support used, providing further confidence that the hydrophobic glass support is not influencing the results.

Below, the onset conditions from this study are compared with results published in the literature. The comparison below focuses mainly on results from five different studies: *Roberts and Hallett* [1968], *Bailey and Hallett*, [2002], *Dymarska et al.* [2006], *Kanji and Abbatt* [2006], and *Zimmermann et al.* [2007]. Some of the experimental conditions from these studies are listed in Table 2.2 for reference.

Table 2.2: Summary of experimental conditions for previously published results

Study	Size range (μm)	Number of particles	Surface Area Range (cm^2)
<i>Current study</i>	1 – 50	$10^2 - 10^3$	$3 \times 10^{-6} - 1 \times 10^{-2}$
<i>Roberts and Hallett, [1968]</i>	0.5 – 3	$10^1 - 10^4$	$8 \times 10^{-8} - 3 \times 10^{-3}$
<i>Bailey and Hallett, [2002]</i>	5 – 10	Not determined	Not determined
<i>Kanji and Abbatt, [2006]</i>	0.5 – 5	$5 \times 10^2 - 3 \times 10^4$	$9 \times 10^{-5} - 3 \times 10^{-2}$
<i>Dymarska et al., [2006]</i>	1 – 20	$2 \times 10^2 - 8 \times 10^2$	$6 \times 10^{-6} - 1 \times 10^{-2}$
<i>Zimmermann et al., [2007]</i>	1 – 10	Not determined ^a	Not determined ^a

^a *Zimmermann et al. [2007]* spread particles on a silicon plate (5mm×5mm), and the particle density was 100–150 particles/mm². However, the exact fraction of particles activated could not be determined precisely because only a small part of the total silicon plate was imaged.

In Figure 2.8, the ice nucleation results for kaolinite are compared with previous measurements. There have only been two previous studies [*Dymarska et al., 2006; Bailey and Hallett, 2002*] conducted in the same temperature range as these experiments. The data from *Dymarska et al. [2006]* are in agreement with the results presented in this thesis, which is not surprising since the same instrument and experimental protocol were employed. The results from *Bailey and Hallett [2002]*, however, differ from the results presented in this thesis by approximately 10–15% RH_i. These differences may be due to variation in mineral surface area available in the different experiments, variation in particle diameters, or variability due to different experimental techniques or different observation times in the experiments. Also, differences in the source of the kaolinite particles may result in some variability in the interaction of the particles with water.

Hoffer [1961] and *Schuttlefield et al.* [2007] reported that water uptake by kaolinite and montmorillonite varied significantly with the location of the mineral source. These points should be investigated in more detail in future experiments.

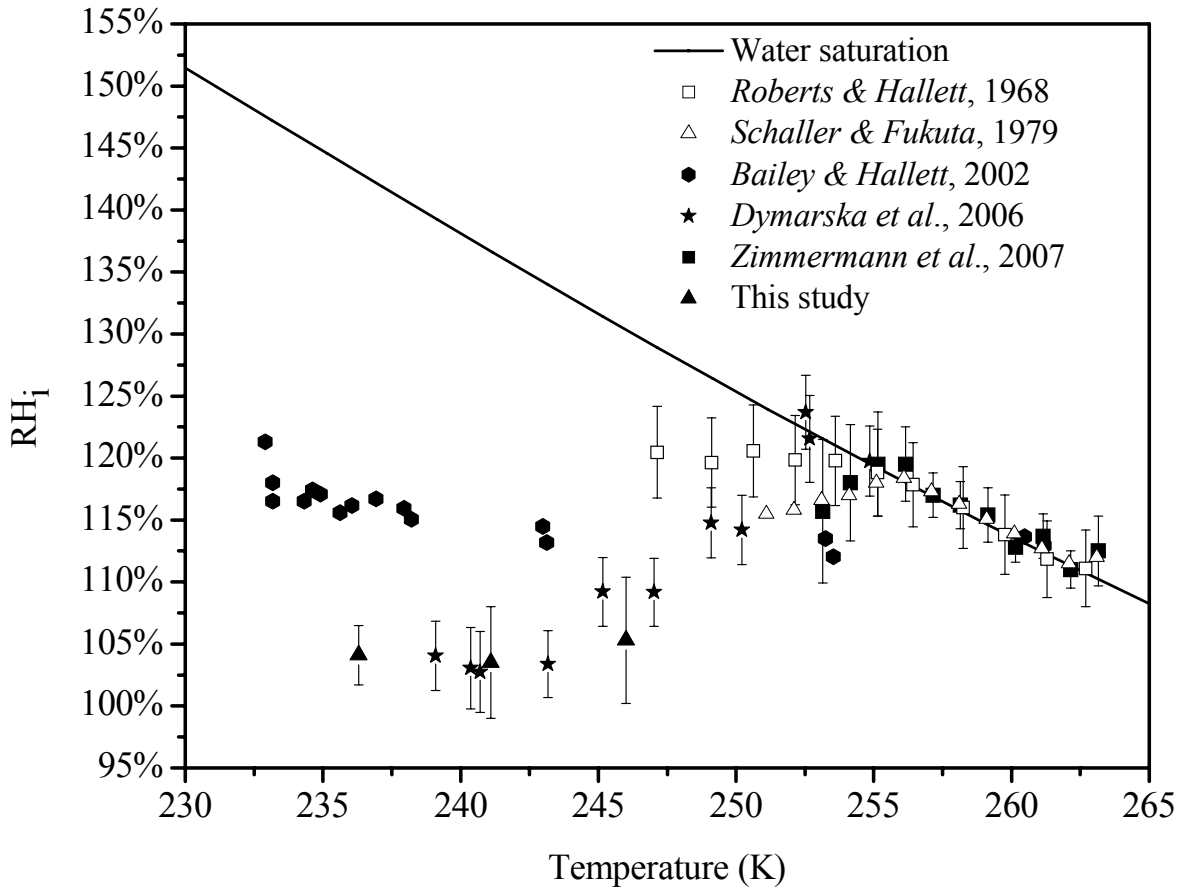


Figure 2.8: Summary of ice nucleation results for kaolinite

Not included in Figure 2.8 are the results from *Salam et al.* [2006]. These authors investigated ice nucleation between 233 K and 258 K using a continuous flow diffusion chamber. They observed that 0.5% of the kaolinite particles activated as ice nuclei even at the lowest supersaturations with respect to ice (close to 100% RH_i). The fraction of particles activated remained almost constant until above 120–130% RH_i , at which point the fraction activated increased sharply. The conditions they report for 0.5% of particles being activated are consistent with the results presented in this thesis.

Considering all of the data from Figure 2.8, the following conclusions seem appropriate. At temperatures above 255 K, ice nucleation does not occur until liquid water saturation is reached. At temperatures below 250 K, all data suggest that kaolinite is an effective ice nucleus (i.e. RH_i values less than water saturation are required for ice nucleation). Quantitatively, however, there are relatively large differences between the different experiments at temperatures below 250 K, as mentioned above.

In Figure 2.9, the ice nucleation results for montmorillonite from these experiments are compared with previous data from *Kanji and Abbatt* [2006] and *Zimmermann et al.* [2007]. The results are consistent with the more recent study by *Zimmermann et al.* [2007] when extrapolated to warmer temperatures, but appear to be inconsistent with the results from *Kanji and Abbatt* [2006].

Not shown in Figure 2.9 are results from *Roberts and Hallett* [1968] and *Salam et al.* [2006]. *Roberts and Hallett* [1968] observed ice nucleation at 248 K and at liquid water saturation when using approximately 10^4 particles, a result that is consistent with those presented in this thesis. *Salam et al.* [2006] found that 1.2% of montmorillonite particles were active ice nuclei even at very small supersaturations with respect to ice ($RH_i \approx 100\%$) over the temperature range of 233 to 258 K. The fraction of activated particles remained almost constant until above approximately 107–115% RH_i , at which point the fraction of activated particles increased sharply. The conditions they report for 1.2% of particles being activated are inconsistent with the data presented for montmorillonite in Figure 2.7 at the warmest temperature (245 K), but consistent at the colder temperatures (236 K and 241 K).

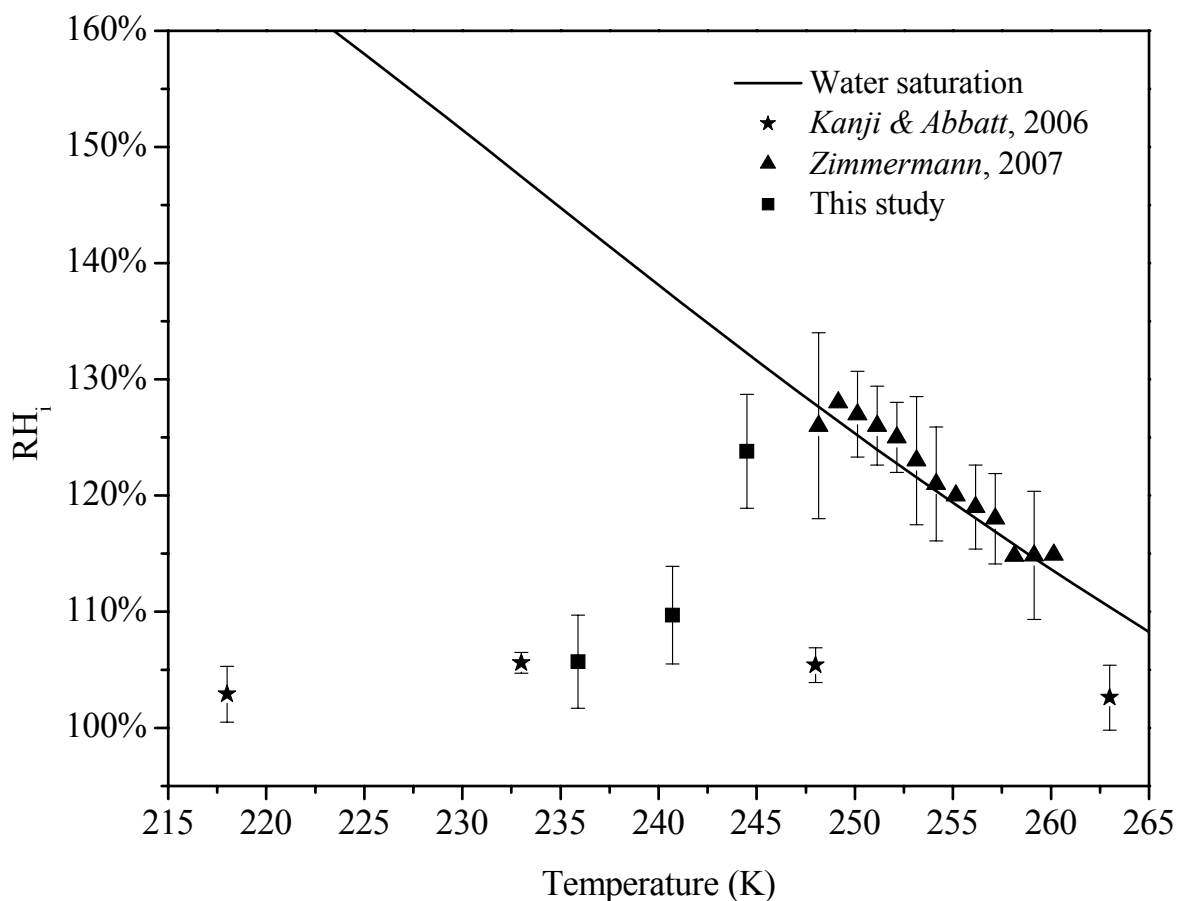


Figure 2.9: Summary of ice nucleation results for montmorillonite

Overall, there appear to be large differences between some of the montmorillonite studies. Some possible reasons for these differences are listed above in the discussion of the kaolinite results. *Kanji and Abbatt* [2006] also presented other reasons why their results may differ from other measurements. First, they suggested a time-dependence may be causing the observed differences, with longer exposure times leading to lower RH_i values required for activation. Second, they suggested that some of the differences may be due to different preparation techniques. *Kanji and Abbatt* [2006] prepared their particles by nebulizing an aqueous suspension of the mineral dust. In contrast, all other studies mentioned above for montmorillonite used a dry deposition technique. Future studies that investigate the effect of these different parameters are needed for a complete

understanding of ice nucleation on mineral particles. At this point, it is reasonable to say that the scientific community's understanding of the ice nucleating properties of montmorillonite remains poor, with results appearing dependent on both the experimental protocol and experimental apparatus.

These are the first measurements of the onset conditions (both RH_i and temperature) for ice nucleation on muscovite. *Mason and Maybank* [1958] reported that muscovite was inactive as an ice nucleus at temperatures above 255 K. This result does not contradict the results for muscovite presented in Figure 2.7, but it should be noted that the temperature range for these experiments does not overlap with the range reported by *Mason and Maybank* [1958].

There are no previous reports of the onset conditions for ice nucleation on quartz particles. *Mason and Maybank* [1958] reported that this mineral was inactive as an ice nucleus at temperatures above 248 K, which is consistent with the results presented for quartz in Figure 2.7.

For calcite, *Roberts and Hallett* [1968] reported one temperature (255 K) and RH_i (120%) at which one particle in 10^4 nucleated ice. Since the temperature measured by these authors is significantly above the temperature range used in these experiments, a direct comparison is not possible; nevertheless, the results from *Roberts and Hallett* [1968] do not contradict the results presented for calcite in Figure 2.7.

2.3.2 Heterogeneous nucleation rates

Onset conditions (RH_i and temperature) may depend on several experimental parameters, such as observation time and surface area available for nucleation. A more useful parameter for describing ice nucleation is the heterogeneous nucleation rate, J_{het} , which allows for a more direct comparison between laboratory studies and for extrapolation to the atmosphere. The heterogeneous nucleation rate is related to onset data through the following equation [*Pruppacher and Klett*, 1997]:

$$J_{\text{het}} = \frac{\omega}{A_s t} \quad (2.5)$$

where ω is the number of ice crystals nucleated, A_s is the total mineral dust surface area available for heterogeneous nucleation, and t is the observation time. At the onset of ice nucleation in these experiments, ω was equal to one. The surface area available for nucleation was determined directly from the optical microscope images using digital imaging software (Northern Eclipse). The observation time for the nucleation event was 20 ± 10 s (equal to the time between image captures). The uncertainty in J_{het} was calculated by considering the uncertainties in A_s and t .

2.3.3 Classical nucleation theory

The applicability of classical nucleation theory to heterogeneous nucleation on mineral dust particles remains to be determined. In fact, some measurements show that for precise predictions, active site theory is required [Hung *et al.*, 2003; Archuleta *et al.*, 2005; Marcolli *et al.*, 2007]. Nevertheless, classical nucleation theory is a relatively convenient and simple way to parameterize laboratory data, and has been used in the past to describe heterogeneous nucleation in atmospheric cloud models [Karcher, 1996; Jensen and Toon, 1997; Jensen *et al.*, 1998; Karcher *et al.*, 1998; Karcher, 1998; Hung *et al.*, 2003]. The significance of applying classical nucleation theory in order to calculate parameters such as contact angles (θ) lies in the fact that these data can be used to make predictions about ice nucleation for varying particle size, shape, composition, or observation time. These data are necessary to extrapolate laboratory data to the atmosphere and predict ice cloud formation accurately for a variety of conditions. Hence, classical nucleation theory is a reasonable starting point for analyzing the onset data from these experiments.

For this analysis, only the case of deposition freezing is considered. As a result, contact angles were not reported for any nucleation data where the onset conditions surpassed or overlapped the liquid water saturation line, since in these cases nucleation may have occurred by either deposition or condensation freezing, as discussed previously.

According to classical nucleation theory, the rate of heterogeneous nucleation by deposition freezing is defined as [Pruppacher and Klett, 1997]:

$$J_{\text{het}} = A \cdot \exp \frac{-\Delta F_{\text{g,het}}}{kT} \quad (2.6)$$

where A is the pre-exponential factor in units of $\text{cm}^{-2} \text{s}^{-1}$, $\Delta F_{\text{g,het}}$ is the free energy of formation of the critical embryo in J, k is the Boltzmann constant in J K^{-1} , and T is the temperature in K. Assuming that an ice embryo on a curved solid substrate can be described as a spherical cap model, the free energy of formation of the critical embryo is given by [Pruppacher and Klett, 1997]:

$$\Delta F_{\text{g,het}} = \frac{16\pi M_w^2 \sigma_{i/v}^3}{3[RT\rho \ln S_i]} \cdot f(m,x) \quad (2.7)$$

where M_w is the molecular weight of water in g mol^{-1} , $\sigma_{i/v}$ is the surface tension at the ice-vapour interface in mJ m^{-2} , R is the universal gas constant in $\text{J mol}^{-1} \text{K}^{-1}$, ρ is the density of ice in g cm^{-3} , S_i is the supersaturation ratio with respect to an ice surface, $f(m,x)$ is the geometric factor, m is the compatibility parameter for ice on a solid substrate, and x is the ratio of the radius of the substrate to the radius of spherical ice germ. The compatibility parameter, m , is equal to $\cos\theta$, where θ is the contact angle between the critical ice nucleus and the mineral surface.

Assuming the radius of the substrate to be much larger than the radius of the ice germ (a good approximation under the experimental conditions), $f(m,x)$ is defined as follows [Pruppacher and Klett, 1997]:

$$f(m,x) = \frac{m^3 - 3m + 2}{4} \quad (2.8)$$

To calculate θ , the free energy of formation of the crucial embryo was calculated from the experimentally determined J_{het} values using Equation 2.6, assuming a pre-

exponential term (A) equal to $10^{25} \text{ cm}^{-2} \text{ s}^{-1}$ [Pruppacher and Klett, 1997]. Then, θ was calculated using Equations 2.7 and 2.8, assuming the density of ice (ρ) is 0.92 g cm^{-3} [CRC, 2001-2002], M_w is $18.015 \text{ g mol}^{-1}$, and $\sigma_{i/v}$ equals $106 \pm 5 \text{ mJ m}^{-2}$ [Pruppacher and Klett, 1997]. For $\sigma_{i/v}$, the surface tension appropriate for hexagonal ice was used. Recent work has shown that cubic ice is the first phase to nucleate when homogeneous nucleation dominates [Murray *et al.*, 2005; Murray and Bertram, 2006], but further research is needed to determine if this also the case for heterogeneous nucleation.

Table 2.3 lists the nucleation rates and contact angles determined from the onset data. The uncertainties in the surface area and observation time were used to calculate upper and lower limits for J_{het} and θ . The data show that the experiments are typically sensitive to values of J_{het} ranging from 60 to $1100 \text{ cm}^{-2}\text{s}^{-1}$, and contact angles ranging from 0° to 30° . The contact angle results are also plotted as a function of temperature in Figure 2.10. The data show that for efficient ice nuclei such as muscovite and kaolinite, the contact angles are small (less than 15°). For poor ice nuclei such as quartz and calcite, the contact angles are larger (greater than 20°). The contact angles measured for montmorillonite were less than 15° at temperatures below 241 K, and greater than 20° at higher temperatures. These data may be useful for future modeling studies of ice nucleation in the atmosphere and for comparing results between different laboratories.

Table 2.3: J values and contact angles for all five minerals studied.

Mineral	Temp. (K)	RH _i (%)	J _{het, low} (cm ⁻² s ⁻¹)	J _{het} (cm ⁻² s ⁻¹)	J _{het, up} (cm ⁻² s ⁻¹)	θ _{lower} (°)	θ (°)	θ _{upper} (°)
Kaolinite	246.1	105 ± 5	100	170	370	5.3	9.7	13.7
Kaolinite	241.1	104 ± 5	100	160	350	2.5	7.8	12.2
Kaolinite	236.4	104 ± 2	70	110	240	3.4	9.2	13.0
Muscovite	246.2	107 ± 5	280	470	1030	7.2	10.7	14.5
Muscovite	241.3	106 ± 6	700	1100	2400	5.6	9.5	14.0
Muscovite	237.0	102 ± 2	150	240	540	0.7	6.2	11.1
Montmorillonite	244.6	124 ± 5	140	230	500	19.8	22.4	24.8
Montmorillonite	240.8	110 ± 4	260	440	960	11.1	14.4	17.3
Montmorillonite	236.0	106 ± 4	280	470	1020	7.8	12.0	15.4
Quartz	243.9	133 ± 1	110	180	400	–	–	–
Quartz	238.7	137 ± 3	100	170	380	24.7	27.2	29.6
Quartz	234.0	136 ± 4	150	240	530	23.9	26.4	28.8
Calcite	244.1	130 ± 3	190	310	680	–	–	–
Calcite	238.9	135 ± 3	80	130	280	24.0	26.5	28.9
Calcite	234.2	132 ± 6	40	60	140	22.5	25.0	27.5

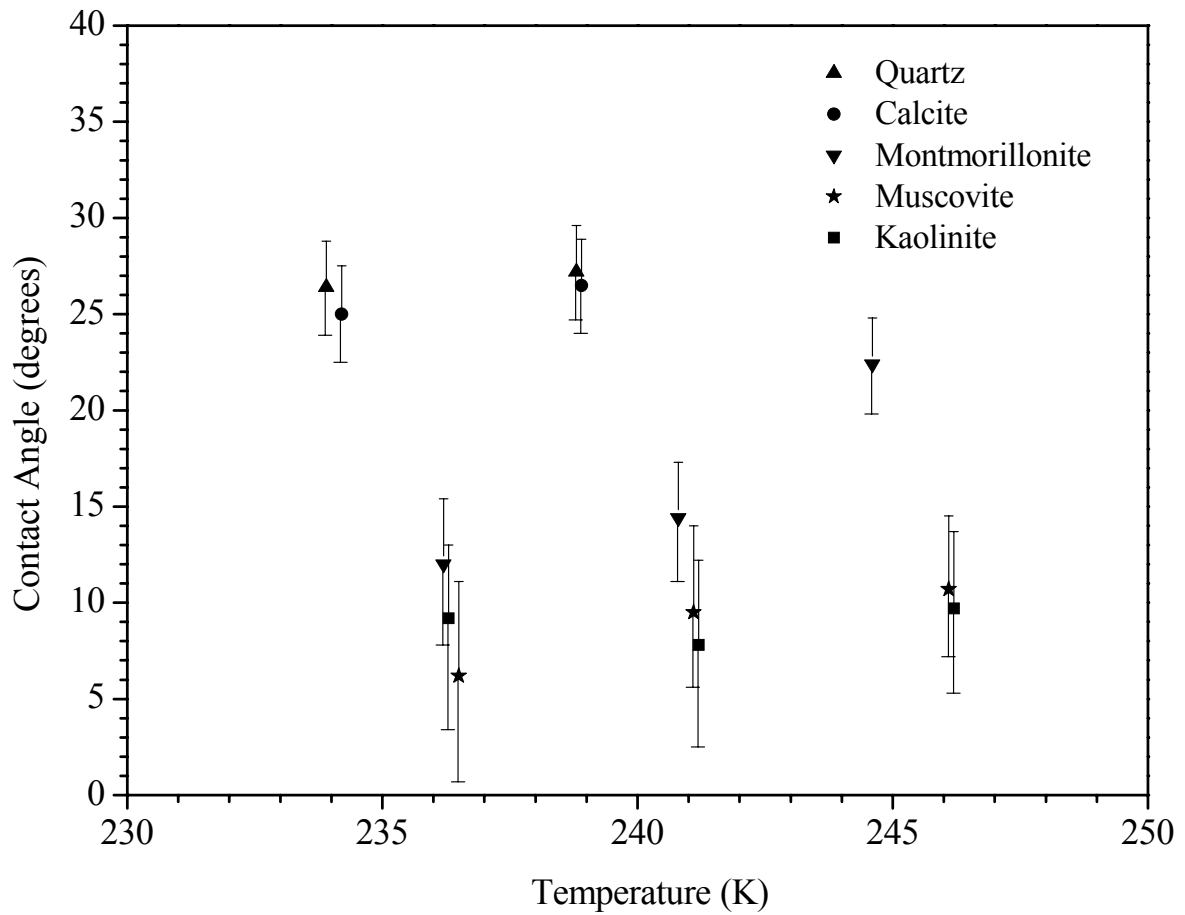


Figure 2.10: Contact angle as a function of temperature for each mineral studied.

3. The effects of sulphuric acid and ammonium sulphate coatings on the ice nucleating properties of kaolinite

3.1 Introduction

When first emitted into the atmosphere, mineral dust particles are likely uncoated. During their lifetime in the atmosphere, which can be hours to weeks depending on particle size [Seinfeld and Pandis, 1998], mineral dusts can become coated with inorganic and/or organic material [Usher *et al.*, 2003]. The following chapter summarizes an investigation into the effects of H_2SO_4 and $(\text{NH}_4)_2\text{SO}_4$ coatings on the ice nucleating properties of mineral dust particles. This research should be useful when trying to determine if anthropogenic emissions of gases such as SO_2 and NH_3 affect climate by “poisoning” natural ice nuclei such as mineral dust.

Additional motivation for this study comes from field measurements made in the Arctic that showed that sulphate coatings drastically decrease the ice nucleating properties of aerosol particles. Borys [1989] reported that the fraction of ice nucleating particles in Arctic haze, which is composed of a wide variety of pollutants including sulphate, was 10 to 1000 times smaller than in Arctic aerosol unaffected by pollution.

This investigation focuses on the ice nucleating properties of kaolinite particles in the presence and absence of H_2SO_4 and $(\text{NH}_4)_2\text{SO}_4$ coatings at temperatures between 233 and 247 K, a temperature range relevant for the troposphere. Prior to this work, there have only been two studies that investigate the effect of H_2SO_4 coatings on the ice nucleating properties of mineral dust particles at temperatures relevant for the troposphere. Knopf and Koop [2006] studied the ice nucleating properties of Arizona test dust (ATD) with and without coatings of H_2SO_4 over the temperature range 197–260 K, and concluded that there was no significant difference between coated and uncoated particles. Archuleta *et al.* [2005] studied ice nucleation on aluminum oxide, amorphous aluminum silicate, iron oxide and Asian dust with and without coatings of H_2SO_4 over the temperature range 213–228 K. Based on their results, they concluded that treatment with H_2SO_4 can either increase or decrease the onset conditions for ice nucleation, depending on the mineral. There have also been two studies of the ice nucleating

properties of mineral dust particles coated with $(\text{NH}_4)_2\text{SO}_4$ [Zuberi *et al.*, 2002; Hung *et al.*, 2003], but in neither case were the ice nucleating properties of the uncoated particles determined, so a direct comparison between uncoated and coated results was not possible. Also related, Georgii [1963] showed that gases such as NH_3 and NO_2 can reduce the ice nucleation ability of atmospheric aerosol particles, while Salam *et al.* [2007] observed that exposure to ammonia gas enhanced the activation of montmorillonite particles as ice nuclei.

Given the dearth of information on the ice nucleating properties of coated mineral dusts, experiments were conducted to determine the onset conditions for kaolinite particles coated with either H_2SO_4 or $(\text{NH}_4)_2\text{SO}_4$. This chapter summarizes the results for coated particles and compares them to those for uncoated particles. Additionally, differences between the results from this study and previously published measurements are discussed in light of varying particle size, coating thickness, and nature of the mineral.

3.2 Experimental

3.2.1 Overview

The technique used in the following investigation has been described in detail in Chapter 2. Here, a brief overview of the technique is provided, with an emphasis on the experimental conditions and procedures specific to the measurements made for H_2SO_4 and $(\text{NH}_4)_2\text{SO}_4$ coated kaolinite particles.

The apparatus used in this study consisted of an optical microscope coupled to a flow-cell (see Figure 2.1, page 16) in which the humidity and temperature could be accurately controlled. Mineral dust particles were deposited on the bottom surface of the flow cell and the relative humidity with respect to ice (RH_i) inside the cell was slowly increased. Ice crystal formation was observed with a reflected-light microscope (Zeiss Axiotech 100) equipped with a $10\times$ objective lens. From these measurements, the onset conditions (temperature and relative humidity) for ice nucleation were determined.

3.2.2 Sample preparation

The uncoated kaolinite particles were prepared by first mixing kaolinite in high-purity water (1% kaolinite by mass of water) to create a suspension. The suspension was stirred and then placed in an ultrasonic bath for 10 minutes. To deposit the particles on the glass slide, the suspension was passed through a nebulizer using high-purity N₂ (99.999%) as a carrier gas. The flow from the nebulizer was directed at the hydrophobic glass slide and droplets containing the particles were deposited on the surface of the slide upon impact. Any water then evaporated, leaving behind the kaolinite particle. The coated kaolinite particles were prepared by mixing the kaolinite and coating material in high-purity water (1% kaolinite and 0.2% coating material by mass in water). This suspension was then stirred and placed in the ultrasonic bath prior to nebulization. The estimated weight fraction of the coatings on particles produced from these suspensions was 0.167. The optical resolution limit of the microscope was $\sim 1 \mu\text{m}$, and a typical sample held between 100 and 1000 individual particles. Shown in Figure 3.1 is an image of kaolinite particles coated with H₂SO₄ deposited on the hydrophobic slide, just prior to an ice nucleation experiment.

It should be noted that the results from the ice nucleation experiments using coated mineral dust particles were compared to results from uncoated particles using the sample preparation procedure outlined above, not the dry deposition procedure described in Chapter 2.

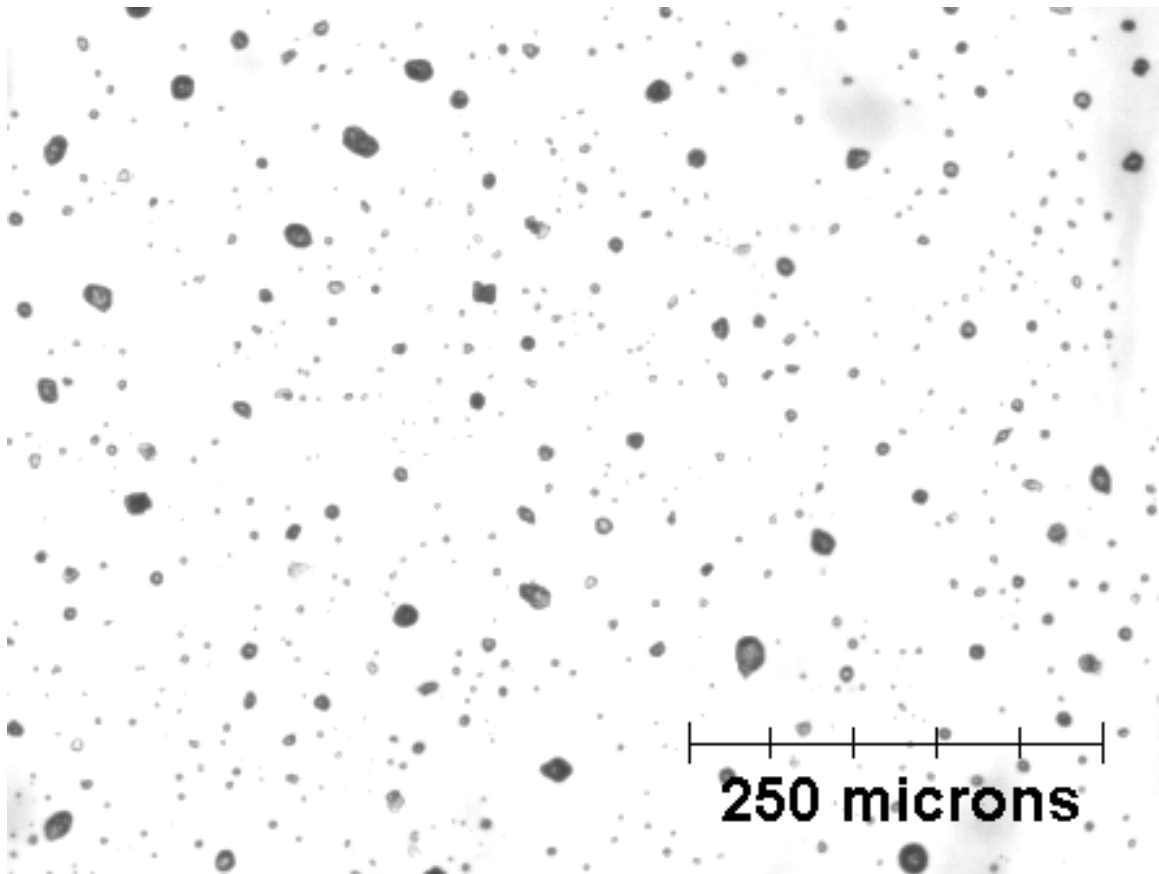


Figure 3.1: Image of H_2SO_4 -coated kaolinite particles prior to an ice nucleation experiment, collected using an optical microscope with a $10\times$ objective.

3.2.3 Coated particle characterization

Using the Northern Eclipse software package, the average sizes of the coated and uncoated particles used in this investigation were determined. Based on an analysis of all the particles studied and assuming a normal distribution of particle size, the mean diameters for the uncoated particles, H_2SO_4 particles and $(\text{NH}_4)_2\text{SO}_4$ particles were 7.7 μm , 7.8 μm and 6.9 μm with standard deviations of 5.3 μm , 5.7 μm and 5.0 μm , respectively.

The thicknesses of the coatings were estimated based on the measured particle sizes and compositions, assuming a spherical core shell model (a kaolinite core surrounded by a uniform H_2SO_4 coating). According to these calculations, under dry conditions ($<1\%$ RH_i) a kaolinite core with a diameter of 15 μm will have a 0.7 μm coating, and a 5 μm core will have a coating of 0.2 μm , representing several hundred sulphate layers covering the surface of the particle.

To further characterize the thickness of the coatings, the change in particle size was monitored as the relative humidity with respect to water (RH_w) was increased from $<1\%$ to 95% at 255 K. These measurements were only meant to provide an additional rough estimate of the coating thickness. For these studies, a Zeiss Axiotech 100 transmitted-light microscope equipped with a 50 \times objective lens was used. Shown in Figure 3.2 are images of two kaolinite particles coated with H_2SO_4 at $<1\%$ and 95% RH_w . From the change in size, the total amount of water adsorbed when cycling between $<1\%$ and 95% RH_w was estimated using the thermodynamic model presented by Clegg *et al.* [1998]. From this, the amount of H_2SO_4 in each particle and thus the thicknesses of the H_2SO_4 coatings under dry conditions were estimated, again assuming a core shell model. Measurements made for 15 individual particles yielded an average weight fraction for the coating of 0.12 ± 0.07 . The uncertainty in this value derives from the uncertainty in the relative humidity measurements.

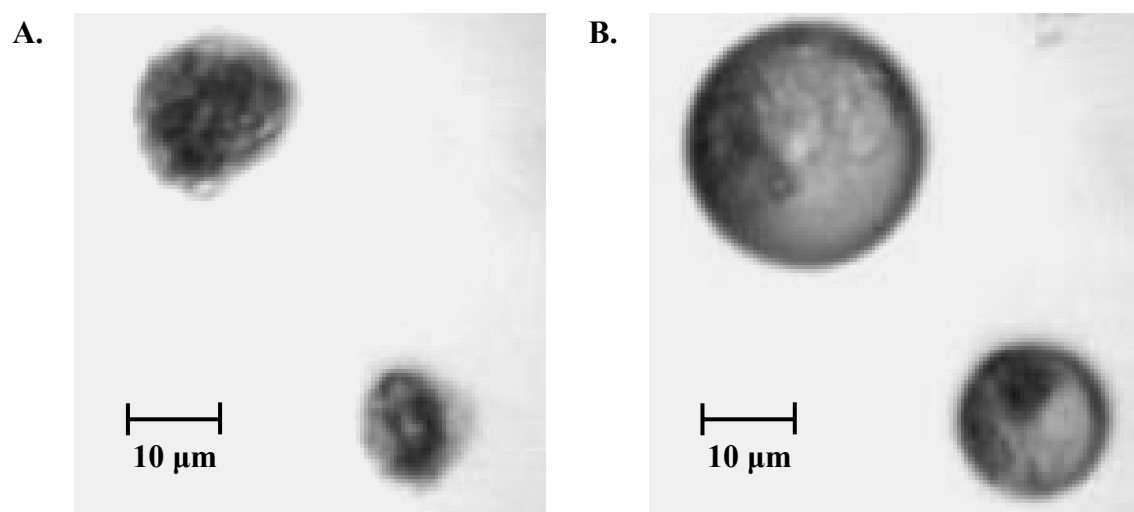


Figure 3.2:

(A) Image of two selected kaolinite particles coated with H_2SO_4 at $\text{RH}_w < 1\%$.

(B) Image of the same two kaolinite particles coated with H_2SO_4 at $\text{RH}_w = 95\%$.

3.3 Results and Discussion

3.3.1 Uncoated kaolinite particles

The total surface area of mineral dust deposited in any particular experiment ranged from 1×10^{-4} to $2 \times 10^{-3} \mu\text{m}^2$. Over this narrow range, the limited data suggest that the onset results did not depend on the surface area. To illustrate this point, onset data for coated and uncoated kaolinite particles recorded at a temperature of 244 K are presented in Figure 3.3. Each point in this figure corresponds to one freezing experiment. Since no clear dependence on surface area was observed, an average and standard deviation for the onset conditions is reported for each temperature. Since approximately the same surface area of mineral was used in the uncoated and coated experiments, the results should be directly comparable.

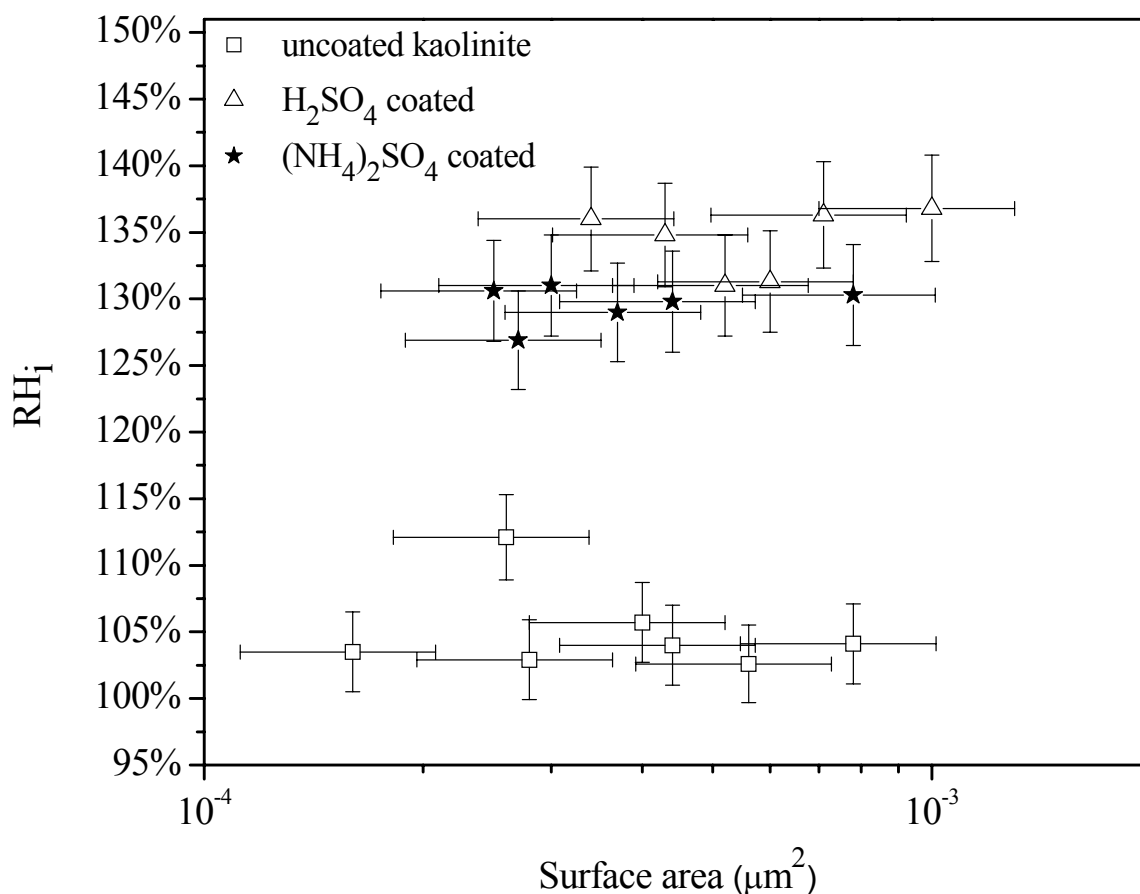


Figure 3.3: Onset RH_i as a function of surface area for uncoated and coated kaolinite particles at 244 K.

The onset results for uncoated kaolinite particles are shown in Figure 3.4. The data show that only a small supersaturation ($<110\%$ RH_i) is required for an ice nucleation event to occur in these experiments. The results obtained here are in excellent agreement with results presented in Chapter 2 for uncoated kaolinite particles. It should be noted, however, that the method of sample preparation in the current experiments differs from the method described in Chapter 2. In the current study, particles were produced by nebulizing a suspension of kaolinite in pure water. The water was then allowed to evaporate, leaving behind the solid kaolinite. By contrast, in Chapter 2 the kaolinite particles were not exposed to an aqueous solution; they were dry when deposited on the

slides. The agreement between the current results and the results from Chapter 2 suggests that the preparation method does not significantly impact the results.

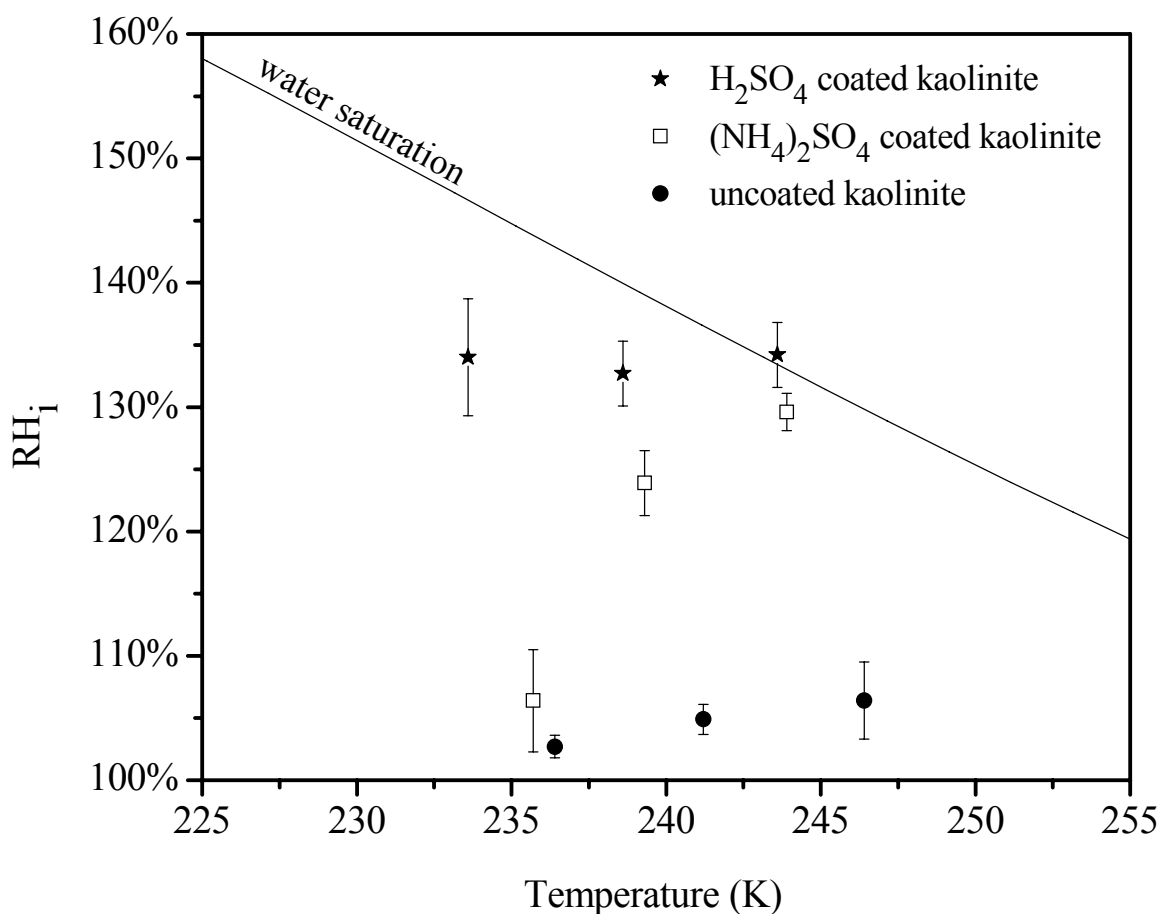


Figure 3.4: Summary of ice nucleation results for coated and uncoated kaolinite particles

3.3.2 H_2SO_4 coated kaolinite particles

Onset results for kaolinite particles coated with H_2SO_4 are also shown in Figure 3.4. In contrast to the uncoated results, the H_2SO_4 coated particles required much higher supersaturations before ice nucleation occurred. The data show that H_2SO_4 coatings drastically altered the ice nucleating ability of kaolinite particles, increasing the RH_i required to initiate ice nucleation by approximately 30%.

Before discussing a possible explanation for the shift in the ice nucleating ability of H_2SO_4 coated particles, the composition of the H_2SO_4 coatings during the ice nucleation experiments must be discussed. Shown in Figure 3.5 are the trajectories used in these experiments and the concentrations of the H_2SO_4 coatings, assuming the vapour is in equilibrium with the aqueous phase. The coloured lines represent RH_i and temperature conditions at which the compositions of the coatings are 10, 20, and 30 wt% H_2SO_4 (the remainder being H_2O), calculated using the model of *Clegg et al.* [1998]. This figure illustrates that the H_2SO_4 coatings are concentrated aqueous solutions (approximately 30 wt% H_2SO_4 at $\text{RH}_i = 100\%$) and that an increase in RH_i results in a decrease of the H_2SO_4 concentration in the solutions surrounding the particles.

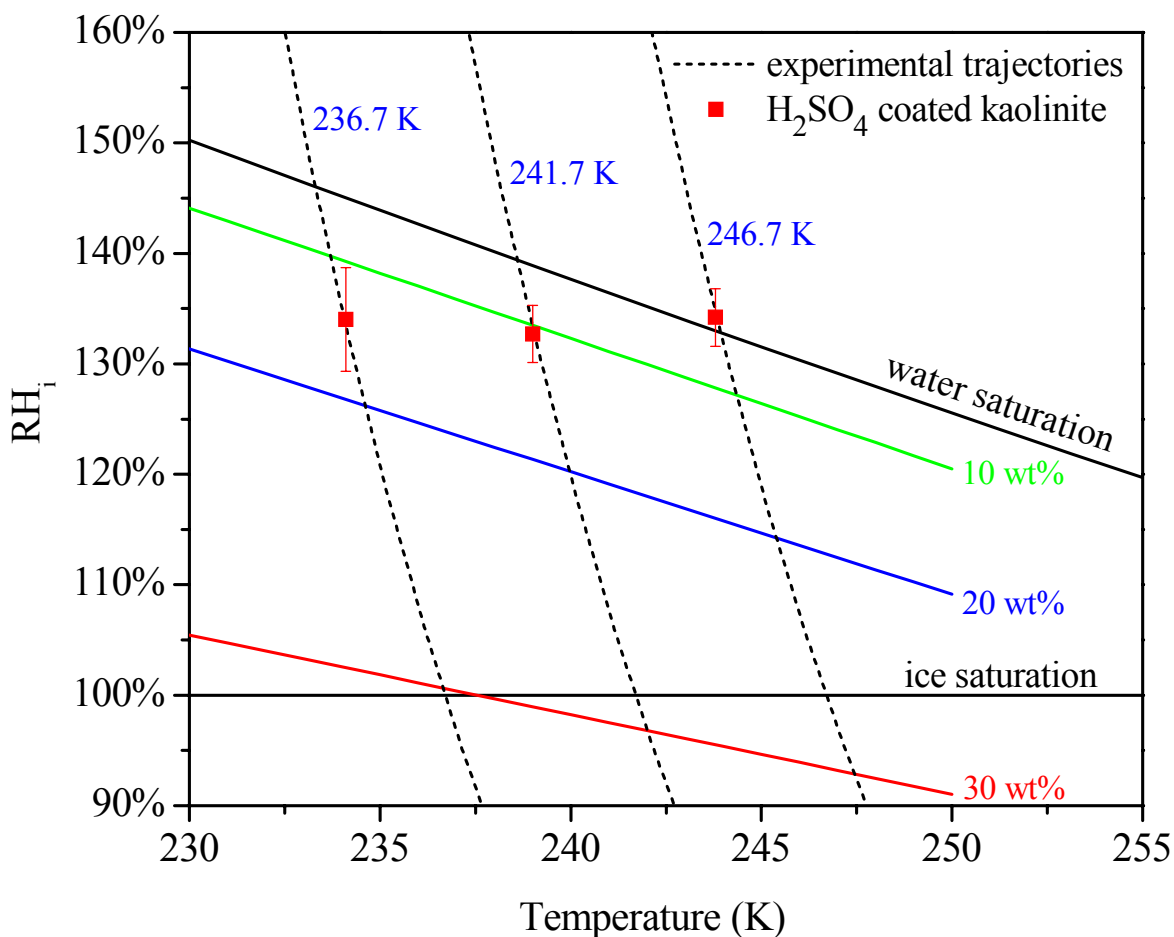


Figure 3.5: Experimental trajectories and lines of constant droplet composition (in wt% H_2SO_4).

It is possible that the poor ice nucleating ability of kaolinite particles coated with H₂SO₄ may be a direct result of the organization of sulphate anions at the solid-aqueous interface. Kaolinite is a 1:1 layered clay mineral whose unit cell is best described as layers of aluminosilicate sheets held together by hydrogen bonds. The “top” surface of these sheets is a gibbsite-like surface with exposed hydroxyl groups. The “bottom” surface of these sheets is a siloxane surface with exposed oxygen atoms [Bergaya *et al.*, Brady *et al.*, 1996]. The Point of Zero Charge (defined as the pH at which the net surface charge is zero) for the gibbsite-like surface is approximately 6, while the Point of Zero Charge for the edge surfaces is approximately 7–8 [Stumm, 1992]. For this discussion, the focus is on the gibbsite-like surface and the edge surface, since the siloxane surface is thought to be rather hydrophobic and hence not a good site for ice nucleation. As mentioned above, the H₂SO₄ coatings in these experiments are very concentrated. The pH of the H₂SO₄ solutions coating the kaolinite particles was calculated to be close to or below 0 under the experimental conditions. As a result, the kaolinite particles should exhibit highly protonated, positively charged surfaces with a proton surface density $\sim 1.2 \times 10^{14} \text{ cm}^{-2}$ [Stumm, 1992; Zhou and Gunter, 1992]. Sulphate is known to strongly interact with mineral surfaces under these conditions [Ali and Dzombak, 1996]. Under these conditions, sulphate anions will likely be attracted to the positively charged kaolinite surface and potentially block ice nucleation sites, which could explain the higher onset RH_i values observed in the experiments with H₂SO₄ coatings. A strong interaction between sulphate anions and positively charged kaolinite surfaces is also consistent with several spectroscopic studies that have shown that sulphate can be involved in strong mono- or bi-dentate chemisorbed complexes with surface protonated hydroxyl groups on iron and aluminum oxide or hydroxide surfaces [Hug, 1997; Peak *et al.*, 1999; Wijnja and Schulthess, 2000; Fukushi and Sverjensky, 2007; Zhang and Peak, 2007]. Future experiments that focus on the partitioning of the sulphate group to the solid-aqueous interface would be helpful, as would investigations into how the arrangement of water molecules close to the kaolinite surface is perturbed by the presence of H₂SO₄.

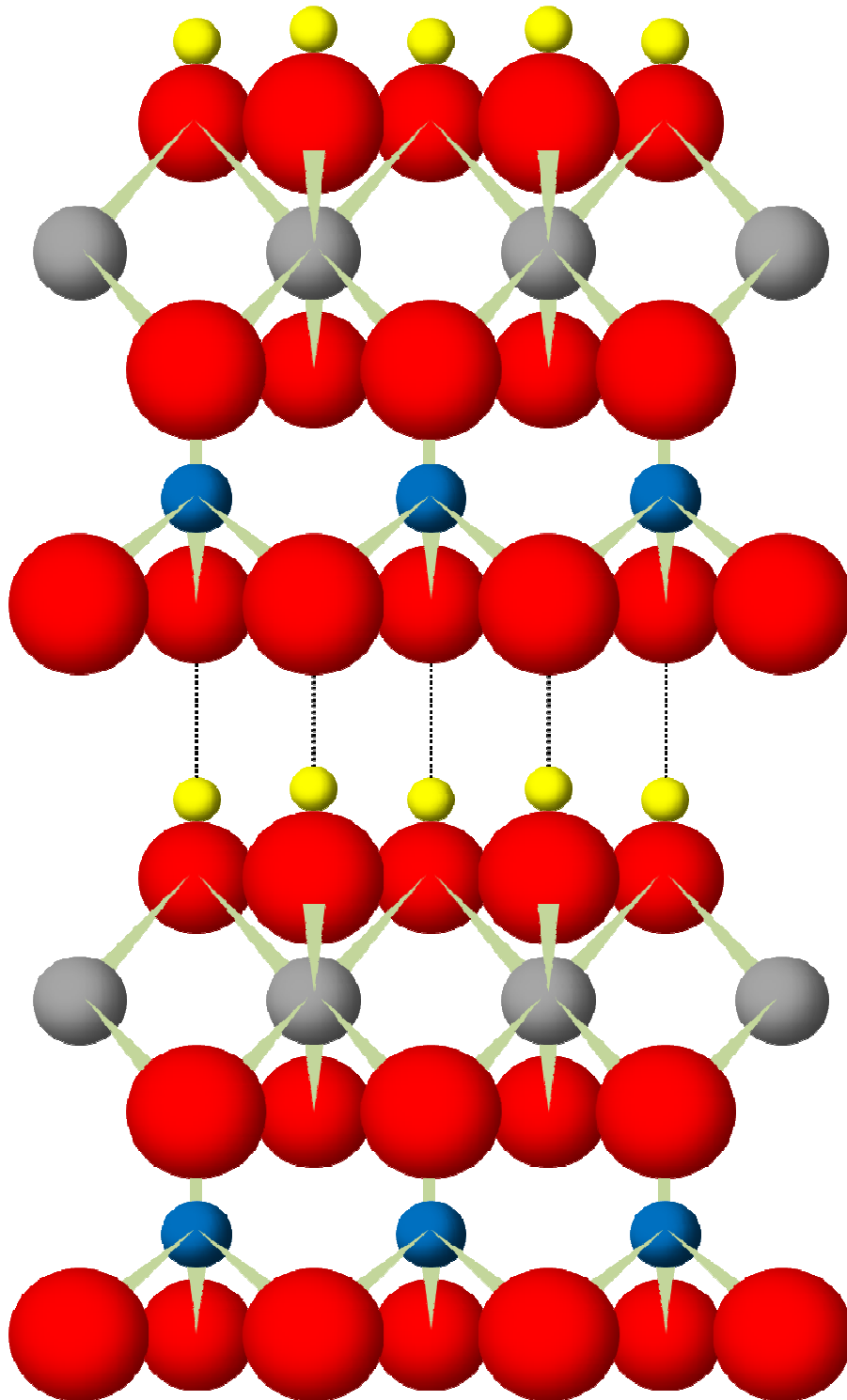


Figure 3.6: The crystal structure of kaolinite. Red = oxygen (O^{2-}), grey = aluminum (Al^{3+}), blue = silicon (Si^{4+}), yellow = hydrogen (H^+). Dotted lines represent hydrogen bonds holding two alumina-silicate sheets together.

As mentioned in the introduction to this chapter, there have only been two previous studies of the effects of H_2SO_4 coatings on mineral dust particles. *Knopf and Koop* [2006] studied ATD particles with and without H_2SO_4 coatings, but they did not observe significant differences due to the coatings. A possible explanation for this apparent discrepancy with the data presented in this chapter may be due to the nature of the minerals studied. For example, perhaps the ATD samples studied by *Knopf and Koop* [2006] contained very little kaolinite or very little kaolinite surface was exposed for ice nucleation. *Archuleta et al.* [2005] studied different oxides, with and without H_2SO_4 coatings. For aluminum oxide and iron oxide, no statistical difference was observed between uncoated and coated particles at 228 K. For amorphous aluminum silicate at the same temperature, they reported that the RH_i required for formation of ice on 1% of 50 nm particles was 10.6% higher for the coated particles. Again, the difference between the results presented in this chapter and the measurements of *Archuleta et al.* [2005] may be due to the different minerals studied. Alternatively, the differences may be related to experimental conditions. For example, *Archuleta et al.* [2005] studied particles with three different monodispersed size distributions centered on 50, 100 and 200 nm, while this study investigated much larger particles. Also, the coatings used by *Archuleta et al.* [2005] were between 2.9 and 7.1 layers thick, which are much smaller than the calculated coating thicknesses for these experiments.

3.3.3 $(\text{NH}_4)_2\text{SO}_4$ coated kaolinite particles

The onset results for $(\text{NH}_4)_2\text{SO}_4$ coated particles are also shown in Figure 3.4. At 240 and 245 K, the RH_i values at the onset of ice nucleation are significantly higher than the uncoated case. However, at 236 K, the coated particles are just as efficient at nucleating ice as the uncoated kaolinite particles. Clearly, the $(\text{NH}_4)_2\text{SO}_4$ coatings are influencing the ice nucleating ability of the kaolinite particles much differently than the H_2SO_4 coatings.

A possible explanation for this difference may be related to the phase (i.e. solid or liquid) of the coatings. For the H_2SO_4 coatings, ice nucleation occurs on a kaolinite particle coated with an aqueous solution. This is not necessarily the case for $(\text{NH}_4)_2\text{SO}_4$

coatings, which can undergo deliquescence and crystallization. Deliquescence occurs when the solid coating absorbs surrounding water vapour and dissolves into a solution at high relative humidity. Crystallization occurs when the supersaturated aqueous coating precipitates to form a solid at low relative humidity. Thus, depending on the temperature and the relative humidity, the $(\text{NH}_4)_2\text{SO}_4$ coating may be solid or liquid. This can complicate the situation, since solid $(\text{NH}_4)_2\text{SO}_4$ is expected to be a good ice nucleus under certain conditions [Zuberi *et al.*, 2002; Abbatt *et al.*, 2006; Shilling *et al.*, 2006]. The phase of the coating is discussed in more detail below.

Figure 3.7 illustrates the possible phase behaviour of an $(\text{NH}_4)_2\text{SO}_4$ coating during a typical freezing experiment. The experiments first start at a very low relative humidity ($\text{RH}_i < 1\%$). Under these conditions, the $(\text{NH}_4)_2\text{SO}_4$ particles are expected to be crystalline, based on previously reported values for the efflorescence relative humidity of pure $(\text{NH}_4)_2\text{SO}_4$ [Martin, 2000] and $(\text{NH}_4)_2\text{SO}_4$ droplets containing kaolinite [Pant *et al.*, 2006]. The RH_i is then increased and above 100% RH_i , ice can nucleate on the solid $(\text{NH}_4)_2\text{SO}_4$ coating. In this case, ice nucleation will occur by deposition freezing, which occurs when water vapour adsorbs onto a solid surface and is transformed into ice [Vali, 1996]. If ice nucleation does not occur, the solid $(\text{NH}_4)_2\text{SO}_4$ coating can take up water at the deliquescence relative humidity (DRH), which is represented by the dashed line in Figure 3.7. Above this relative humidity, the $(\text{NH}_4)_2\text{SO}_4$ coating is a liquid and ice nucleation can occur by immersion freezing.

Based on the discussion above, the data suggest that solid $(\text{NH}_4)_2\text{SO}_4$ coatings are good ice nuclei at approximately 236 K. This is consistent with previous laboratory data that show that solid $(\text{NH}_4)_2\text{SO}_4$ particles are good ice nuclei below 239 K [Zuberi *et al.*, 2002; Abbatt *et al.*, 2006; Shilling *et al.*, 2006].

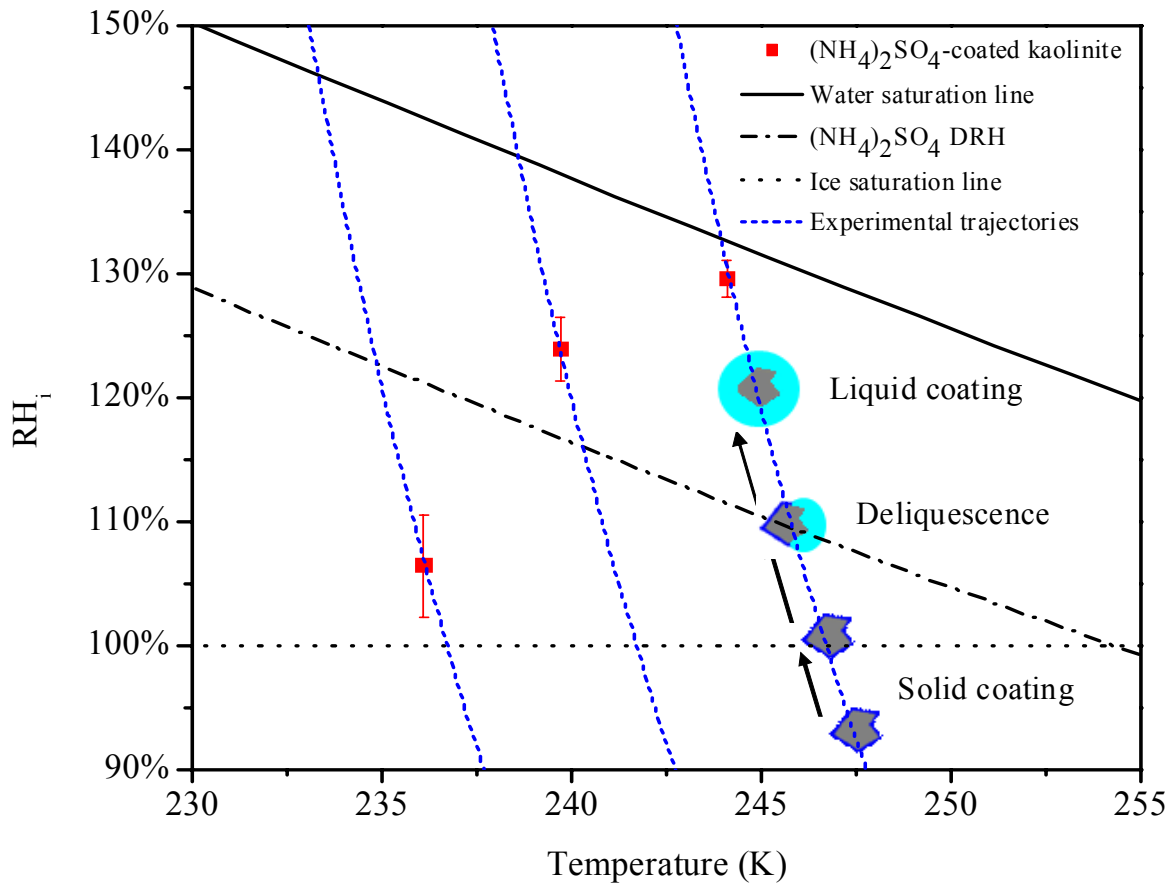


Figure 3.7: Schematic of the possible phase behaviour of an $(\text{NH}_4)_2\text{SO}_4$ coating during a typical freezing experiment

4. Concluding remarks

4.1 Uncoated mineral dust

The ice nucleating properties of five mineral dusts were studied at temperatures ranging from 233 to 247 K. Kaolinite and muscovite, two alumina-silicate clays, were determined to be effective ice nuclei at all temperatures studied. The observed onset of ice nucleation was below 110% RH_i (well below water saturation) for both minerals. Montmorillonite, the third alumina-silicate clay, behaved similarly to kaolinite and muscovite at lower temperatures and was determined to be an effective ice nucleus below 241 K, but a poor ice nucleus at 245 K and above. Quartz and calcite were poor ice nuclei at all temperatures studied. For the temperature range studied, the RH_i values needed to induce ice nucleation on quartz and calcite were approximately 20 to 40% higher than those needed for kaolinite and muscovite. Overall, the data show significant differences in the ice nucleating abilities of the five minerals studied over this temperature range.

The measured onset conditions for the mineral dusts were compared with previously published data. In several cases, there was a lack of quantitative agreement among published work. This can be explained by several factors including the mineral source, the particle size, the surface area available for nucleation, observation and equilibrium times. Future studies that investigate the effects of these different parameters are needed for a complete understanding of ice nucleation on mineral particles.

The heterogeneous nucleation rates (J_{het}) and contact angles (θ) were determined according to classical nucleation theory for all five minerals studied. The contact angles measured for kaolinite and muscovite ranged from 6 to 12°, whereas for quartz and calcite the contact angles ranged from 25 to 27°. For montmorillonite, the contact angles measured below 241 K ranged from 15°, while the contact angle at 245 K was 21°. These data may allow for a more direct comparison between laboratory studies and can be used when modeling ice cloud formation in the atmosphere.

4.2 Coated mineral dust

The ice nucleating properties of kaolinite particles at temperatures ranging from 233 to 247 K change drastically when coated with either H_2SO_4 or $(\text{NH}_4)_2\text{SO}_4$. Uncoated kaolinite particles are effective ice nuclei, but kaolinite particles coated with H_2SO_4 are relatively poor ice nuclei, requiring RH_i values approximately 30% higher than uncoated particles in order to initiate ice nucleation. One possible explanation for this difference is the protonation of the kaolinite surface and the adsorption of sulphate anions onto surface hydroxyl groups resulting in a blocking of ice nucleation sites. The ice nucleating properties of particles coated with $(\text{NH}_4)_2\text{SO}_4$ depend on the temperature: at low temperatures (i.e. 235 K), the ice nucleating ability for $(\text{NH}_4)_2\text{SO}_4$ coated particles is comparable to that of uncoated particles with an onset RH_i of 107%; however, at 240 K and above, the $(\text{NH}_4)_2\text{SO}_4$ coated particles are poor ice nuclei, much like the H_2SO_4 coated particles. The differences in the results obtained for H_2SO_4 and $(\text{NH}_4)_2\text{SO}_4$ may be explained by the deliquescence and efflorescence properties of $(\text{NH}_4)_2\text{SO}_4$.

These initial results support the idea that anthropogenic emissions of SO_2 and NH_3 may influence the ice nucleating properties of mineral dust particles by increasing the relative humidity required for ice nucleation on these particles. This shift in the conditions necessary for ice nucleation may influence the frequency and properties of ice clouds. Calculations using a cloud parcel model are needed to explore this possibility further.

Field measurements made in the Arctic region show a drastic reduction in the number of ice-forming nuclei when sulphate concentrations are high [Borys, 1989]. The results presented in this thesis do not provide information on the change in number of ice nuclei since only the onset conditions for ice nucleation were determined. More work is needed to explain the measurements by Borys [1989], but the results presented herein support the idea that H_2SO_4 and $(\text{NH}_4)_2\text{SO}_4$ coatings can significantly influence the ice nucleating properties of mineral dust particles.

4.3 Suggestions for future work

Several experiments are recommended to further our understanding of mineral dusts and the role they play as ice nuclei in the troposphere:

- (1) The ice nucleating abilities of five uncoated minerals were determined in these studies; however, atmospheric mineral dust has many components of varying concentration. Future experiments to determine the ice nucleating abilities of other major components of mineral dust such as chlorite, corundum, hematite, gypsum and feldspar should be conducted.
- (2) The effects of H_2SO_4 and $(\text{NH}_4)_2\text{SO}_4$ coatings on the ice nucleating ability of dust were only determined for one mineral – kaolinite. Investigations into the effects of sulphate coatings on other mineral dusts will be necessary in order to understand the impact that these chemicals can have on ice cloud formation in the troposphere.
- (3) The effects of different inorganic coatings such as NH_4HSO_4 and NH_4NO_3 on the ice nucleating ability of mineral dust should be investigated.
- (4) The effects of organic coatings and mixed organic-inorganic coatings on the ice nucleating ability of mineral dust should be studied.
- (5) An investigation of the dependence of onset conditions and nucleation rates on particle size and the surface area available for nucleation should be conducted in order to establish more accurate predictions of ice nucleation in the atmosphere.

REFERENCES

- Abbatt, J.P.D., S. Benz, D.J. Cziczo, Z. Kanji, U. Lohmann, and O. Mohler, Solid ammonium sulfate aerosols as ice nuclei: A pathway for cirrus cloud formation, *Science*, 313 (5794), 1770–1773, 2006.
- Ahrens, C.D., *Meteorology Today*, West Publishing Company, St. Paul, 1994.
- Albrecht, B., Aerosols, cloud microphysics and fractional cloudiness, *Science*, 245, 1227–1230, 1989.
- Ali, M.A., and D.A. Dzombak, Competitive sorption of simple organic acids and sulfate on goethite, *Env. Sci. Tech.*, 30, 1061, 1996.
- Andreae, M.O., Climatic effects of changing atmospheric aerosol levels., in *World Survey of Climatology, vol. 16, Future Climates of the World*, edited by A. Henderson-Sellers, pp. 341–392, Elsevier, New York, 1995.
- Anthony, J.W., R.A. Bideaux, K.W. Bladh, and M.C. Nichols, *Handbook of Mineralogy*, Mineral Data Publishing, Tucson, AZ, 1995.
- Archuleta, C.M., P.J. Demott, and S.M. Kreidenweis, Ice nucleation by surrogates for atmospheric mineral dust and mineral dust/sulfate particles at cirrus temperatures, *Atmos. Chem. Phys.*, 5, 2617–2634, 2005.
- Avramov, A., The influence of ice nucleation mode and ice vapor growth on simulation of Arctic mixed-phase clouds, in *Proceeding of the sixteenth ARM science team meeting, March 2006*, Albuquerque, New Mexico, 2006.
- Bailey, M., and J. Hallett, Nucleation effects on the habit of vapour grown ice crystals from -18 to -42 °C, *Quart. J. Roy. Meteor. Soc.*, 128, 1461–1483, 2002.
- Bergaya, F., B.K.G. Theng, and G. Lagaly, *Handbook of clay science*, 2006.
- Berry, L.G., B. Mason, and R.V. Dietrich, *Mineralogy, 2nd ed.*, W.H. Freeman, New York, 1983.
- Borys, R.D., Studies of ice nucleation by Arctic aerosol on AGASP-II, *J. Atmos. Chem.*, 9, 169–185, 1989.
- Cantrell, W., and A.J. Heymsfield, Production of ice in tropospheric clouds – a review, *Bull. Amer. Meteorol. Soc.*, 86 (6), 795–807, 2005.
- Chen, Y.L., S.M. Kreidenweis, L.M. McInnes, D.C. Rogers, and P.J. DeMott, Single particle analyses of ice nucleating aerosols in the upper troposphere and lower stratosphere, *Geophys. Res. Lett.*, 25 (9), 1391–1394, 1998.

- Clegg, S.L., P. Brimblecombe, and A.S. Wexler, Thermodynamic model of the system $\text{H}^+ - \text{NH}_4^+ - \text{SO}_4^{2-} - \text{NO}_3^- - \text{H}_2\text{O}$ at tropospheric temperatures, *J. Phys. Chem. A*, *102* (12), 2137–2154, 1998.
- Cziczo, D.J., D.M. Murphy, P.K. Hudson, and D.S. Thomson, Single particle measurements of the chemical composition of cirrus ice residue during CRYSTAL-FACE, *J. Geophys. Res.*, *109*, D04201, 2004.
- d'Almeida, G.A., A model for Saharan dust transport, *J. Clim. Appl. Meteor.*, *25*, 903–916, 1986.
- d'Almeida, G.A., P. Koepke, and E.P. Shettle, *Atmospheric Aerosols-Global Climatology and Radiative Characteristics*, Hampton, VA, 1991.
- DeMott, P.J., Laboratory studies of cirrus cloud processes, in *Cirrus*, edited by D.K. Lynch, pp. 102–136, Oxford University Press, New York, 2002.
- DeMott, P.J., K. Sassen, M.R. Poellot, D. Baumgardner, D.C. Rogers, S.D. Brooks, A.J. Prenni, and S.M. Kreidenweis, African dust aerosols as atmospheric ice nuclei, *Geophys. Res. Lett.*, *30* (14), 1732, doi:10.1029/2003GL017410, 2003a.
- DeMott, P.J., D.J. Cziczo, A.J. Prenni, D.M. Murphy, S.M. Kreidenweis, D.S. Thomson, R. Borys, and D.C. Rogers, Measurements of the concentration and composition of nuclei for cirrus formation, *Proc. Nat. Acad. Sci. U.S.A.*, *100* (25), 14655–14660, 2003b.
- Duce, R.A., Sources, distributions, and fluxes of mineral aerosols and their relationship to climate, in *Aerosol Forcing of Climate*, edited by R.J. Charlson, and J. Heintzenberg, pp. 43–72, Wiley, Chichester, 1995.
- Dymarska, M., B.J. Murray, L.M. Sun, M.L. Eastwood, D.A. Knopf, and A.K. Bertram, Deposition ice nucleation on soot at temperatures relevant for the lower troposphere, *J. Geophys. Res.*, *111*, D04204, 2006.
- Field, P.R., O. Möhler, P. Connolly, M. Krämer, R. Cotton, A.J. Heymsfield, H. Saathoff, and M. Schnaiter, Some ice nucleation characteristics of Asian and Saharan desert dust, *Atmos. Chem. Phys.*, *6*, 2991–3006, 2006.
- Finlayson-Pitts, B.J., and J.N.J. Pitts, *Chemistry of the Upper and Lower Atmosphere*, Academic Press, San Diego, 2000.
- Fletcher, N.H., *Physics of rain and clouds*, Cambridge University Press, London, 1962.
- Forster, P., V. Ramaswamy, P. Artaxo, T. Berntsen, R. Betts, D.W. Fahey, J. Haywood, J. Lean, D.C. Lowe, G. Myhre, J. Nganga, R. Prinn, G. Raga, M. Schulz, and R.V. Dorland, Changes in Atmospheric Constituents and in Radiative Forcing., in *Climate Change 2007: The Physical Science Basis. Contribution of Working Group I to the Fourth Assessment Report of the Intergovernmental Panel on Climate Change*, edited by S. Solomon, D. Qin, M. Manning, Z. Chen, M. Marquis, K.B. Averyt, M. Tignor, and

H.L. Miller, pp. 129–234, Cambridge University Press, Cambridge, United Kingdom and New York, NY, USA, 2007.

Fukushi, K., and D.J. Sverjensky, A surface complexation model for sulfate and selenate on iron oxides consistent with spectroscopic and theoretical molecular evidence, *Geochim. Cosmochim. Acta*, *71*, 1-24, 2007.

Georgii, H.W., Investigations on the deactivation of inorganic and organic freezing-nuclei, *Z. Angew. Math. Phys.*, *14*, 503-510, 1963.

Girard, E., and J.A. Curry, Simulation of low-level tropospheric clouds during FIRE experiment in May 1998, *J. Geophys. Res.*, *106*, 15139–15154, 2001.

Girard, E., J.-P. Blanchet, and Y. Dubois, Effects of sulphuric acid aerosols on wintertime low-level atmospheric ice crystals, humidity, and temperature at Alert, Nunavut, *Atmos. Res.*, *73*, 131–148, 2005.

Glaccum, R.A., and J.M. Prospero, Saharan aerosols over the tropical North Atlantic - Mineralogy, *Mar. Geol.*, *37*, 295–321, 1980.

Haag, W., and B. Kärcher, The impact of aerosols and gravity waves on cirrus clouds at midlatitudes, *J. Geophys. Res.*, *109*, D12202, doi:10.1029/2004JD004579, 2004.

Hanisch, F., and J.N. Crowley, The heterogeneous reactivity of gaseous nitric acid on authentic mineral dust samples, and on individual mineral and clay mineral components, *Phys. Chem. Chem. Phys.*, *3*, 2474–2482, 2001.

Haywood, J., and O. Boucher, Estimates of the direct and indirect radiative forcing due to tropospheric aerosols: a review, *Rev. Geophys.*, *38* (4), 513–543, 2000.

Heintzenberg, J., K. Okada, and J. Ström, On the composition of non-volatile material in upper tropospheric aerosols and cirrus crystals, *Atmos. Res.*, *41*, 81–88, 1996.

Hoffer, T.E., A laboratory investigation of droplet freezing, *J. Meteorol.*, *18*, 766–778, 1961.

Hug, S.J., *In situ* Fourier Transform infrared measurements of sulfate adsorption on hematite in aqueous solutions, *J. Colloid Interface Sci.*, *188*, 415–422, 1997.

Hung, H.M., A. Malinowski, and S.T. Martin, Kinetics of heterogeneous ice nucleation on the surfaces of mineral dust cores inserted into aqueous ammonium sulfate particles, *J. Phys. Chem. A*, *107* (9), 1296–1306, 2003.

Jensen, E.J., and O.B. Toon, The potential impact of soot particles from aircraft exhaust on cirrus clouds, *Geophys. Res. Lett.*, *24* (3), 249–252, 1997.

Jensen, E.J., O.B. Toon, R.F. Pueschel, J. Goodman, G.W. Sachse, B.E. Anderson, K.R. Chan, D. Baumgardner, and R.C. Miake-Lye, Ice crystal nucleation and growth in

- contrails forming at low ambient temperatures, *Geophys. Res. Lett.*, *25* (9), 1371–1374, 1998.
- Kanji, Z.A., and J.P.D. Abbatt, Laboratory studies of ice formation via deposition mode nucleation onto mineral dust and n-hexane soot samples, *J. Geophys. Res.*, *111*, D16204, 2006.
- Kärcher, B., Aircraft-generated aerosols and visible contrails, *Geophys. Res. Lett.*, *23* (15), 1933–1936, 1996.
- Kärcher, B., R. Busen, A. Petzold, F.P. Schroder, U. Schumann, and E.J. Jensen, Physicochemistry of aircraft-generated liquid aerosols, soot, and ice particles – 2. Comparison with observations and sensitivity studies, *J. Geophys. Res.*, *103* (D14), 17129–17147, 1998.
- Kärcher, B., Physicochemistry of aircraft-generated liquid aerosols, soot, and ice particles – 1. Model description, *J. Geophys. Res.*, *103* (D14), 17111–17128, 1998.
- Kärcher, B., Cirrus clouds in the tropical tropopause layer: Role of heterogeneous ice nuclei, *Geophys. Res. Lett.*, *31*, L12101, doi:10.1029/2004GL019774, 2004.
- Knopf, D.A., and T. Koop, Heterogeneous nucleation of ice on surrogates of mineral dust, *J. Geophys. Res.*, *111*, D12201, 2006.
- Lohmann, U., and J. Feichter, Global indirect aerosol effects: a review, *Atmos. Chem. Phys.*, *5*, 715–737, 2005.
- Lohmann, U., and K. Diehl, Sensitivity studies of the importance of dust ice nuclei for the indirect aerosol effect on stratiform mixed-phase clouds, *J. Atmos. Sci.*, *63*, 968–982, 2006.
- Mangold, A., R. Wagner, H. Saathoff, U. Schurath, C. Gieseemann, V. Ebert, M. Kramer, and O. Möhler, Experimental investigation of ice nucleation by different types of aerosols in the aerosol chamber AIDA: implications to microphysics of cirrus clouds, *Meteorol. Z.*, *14* (4), 485–497, 2005.
- Marculli, C., S. Gedamke, T. Peter, and B. Zobrist, Efficiency of immersion mode ice nucleation on surrogates of mineral dust, *Atmos. Chem. Phys.*, *7*, 5081–5091, 2007.
- Martin, S.T., Phase transitions of aqueous atmospheric particles, *Chem. Rev.*, *100* (9), 3403–3453, 2000.
- Mason, B.J., and J. Maybank, Ice nucleating properties of some natural mineral dusts, *Quart. J. Roy. Meteor. Soc.*, *84*, 235–241, 1958.
- Meyers, M.P., P.J. Demott, and W.R. Cotton, New primary ice nucleation parameterization in an explicit cloud model, *J. Appl. Meteor.*, *31*, 708–721, 1992.

Middlebrook, A.M., L.T. Iraci, L.S. McNeill, B.G. Koehler, M.A. Wilson, O.W. Saastad, M.A. Tolbert, and D.R. Hanson, Fourier Transform-Infrared studies of thin H₂SO₄/H₂O films - formation, water-uptake, and solid-liquid phase-changes, *J. Geophys. Res.*, *98* (D11), 20473–20481, 1993.

Möhler, O., P.R. Field, P. Connolly, S. Benz, H. Saathoff, M. Schnaiter, R. Wagner, R. Cotton, M. Krämer, A. Mangold, and A.J. Heymsfield, Efficiency of the deposition mode ice nucleation on mineral dust particles, *Atmos. Chem. Phys.*, *6*, 3007–3021, 2006.

Murphy, D.M., and T. Koop, Review of the vapour pressures of ice and supercooled water for atmospheric applications, *Quart. J. Roy. Meteor. Soc.*, *131* (608), 1539–1565, 2005.

Murray, B.J., D.A. Knopf, and A.K. Bertram, The formation of cubic ice under conditions relevant to Earth's atmosphere, *Nature*, *434*, 202–205, 2005.

Murray, B.J., and A.K. Bertram, Formation and stability of cubic ice in water droplets, *Phys. Chem. Chem. Phys.*, *8*, 186–192, 2006.

Pant, A., M.T. Parsons, and A.K. Bertram, Crystallization of aqueous ammonium sulfate particles internally mixed with soot and kaolinite: Crystallization relative humidities and nucleation rates, *J. Phys. Chem. A*, *110* (28), 8701–8709, 2006.

Parsons, M.T., J. Mak, S.R. Lipetz, and A.K. Bertram, Deliquescence of malonic, succinic, glutaric, and adipic acid particles, *J. Geophys. Res.*, *109*, D06212, 2004.

Peak, D., R.G. Ford, and D.L. Sparks, An *in situ* ATR-FTIR investigation of sulfate bonding mechanisms on goethite, *J. Colloid Interface Sci.*, *218*, 289–299, 1999.

Peterson, J.T., and C.E. Junge, Source of particulate matter in the atmosphere, in *Man's Impact on Climate*, edited by W. Matthews, W. Kellog, and G.D. Robinson, pp. 310–320, MIT Press, Cambridge, MA, 1971.

Prospero, J.M., Long-range transport of mineral dust in the global atmosphere: Impact of African dust on the environment of the southeastern United States, *Proc. Nat. Acad. Sci. U.S.A.*, *96*, 3396–3403, 1999.

Pruppacher, H.R., and J.D. Klett, *Microphysics of Clouds and Precipitation*, Kluwer Academic Publishers, Dordrecht, 1997.

Roberts, P., and J. Hallett, A laboratory study of the ice nucleating properties of some mineral particulates, *Quart. J. Roy. Meteor. Soc.*, *94*, 25–34, 1968.

Salam, A., U. Lohmann, B. Crenna, G. Lesins, P. Klages, D. Rogers, R. Irani, A. MacGillivray, and M. Coffin, Ice nucleation studies of mineral dust particles with a new continuous flow diffusion chamber, *Aerosol Sci. Technol.*, *40*, 134–143, 2006.

Salam, A., U. Lohmann, and G. Lesins, Ice nucleation of ammonia gas exposed

- montmorillonite mineral dust particles, *Atmos. Chem. Phys.*, 7, 3923–3931, 2007.
- Sassen, K., Indirect climate forcing over the western US from Asian dust storms, *Geophys. Res. Lett.*, 29 (10), 1465, doi:10.1029/2001GL014051, 2002.
- Sassen, K., P.J. DeMott, J.M. Prospero, and M.R. Poellot, Saharan dust storms and indirect aerosol effects on clouds: CRYSTAL-FACE results, *Geophys. Res. Lett.*, 30 (12), 1633, doi:10.1029/2003GL017371, 2003.
- Sassen, K., Dusty ice clouds over Alaska, *Nature*, 434, 456, 2005.
- Schuttlefield, J.D., D. Cox, and V.H. Grassian, An investigation of water uptake on clays minerals using ATR-FTIR spectroscopy coupled with quartz crystal microbalance measurements, *J. Geophys. Res.*, 112, D21303, doi:10.1029/2007JD008973, 2007.
- Schütz, L., and M. Sebert, Mineral aerosols and source identification, *J. Aerosol. Sci.*, 18 (1), 1–10, 1987.
- Schütz, L., in *Paleoclimatology and Paleometeorology: Modern and Past Patterns of Global Atmospheric Transport*, edited by M. Leinen, and M. Sarnthein, pp. 359–384, Kluwer, Dordrecht, The Netherlands, 1989.
- Schütz, L., in *Proceedings of the Alfred-Wegener-Conference: Sediment and Aerosol*, edited by W.v. Hoyningen-Huene, and G. Tetzlaff, pp. 9–13, Leipzig, Germany, 1997.
- Seinfeld, J.H., and S.N. Pandis, *Atmospheric Chemistry and Physics from Air Pollution to Climate Change*, John Wiley & Sons, Inc., New York, 1998.
- Shilling, J.E., T.J. Fortin, and M.A. Tolbert, Depositional ice nucleation on crystalline organic and inorganic solids, *J. Geophys. Res.*, 111, D12204, 2006.
- Sokolik, I., D. Winker, G. Bergametti, D. Gillette, G. Carmichael, Y. Kaufman, L. Gomes, L. Schuetz, and J. Penner, Introduction to special section: Outstanding problems in quantifying the radiative impacts of mineral dust, *J. Geophys. Res.*, 106 (D16), 18015–18027, 2001.
- Stumm, W., *Chemistry of the solid-water interface*, Willey-Interscience, New York, 1992.
- Tegen, I., and I. Fung, Contribution to the atmospheric mineral aerosol load from land surface modification, *Journal of Geophysical Research*, 100 (D9), 18707–18726, 1995.
- Toon, O.B., African dust in Florida clouds, *Nature*, 424, 623–624, 2003.
- Twohy, C.H., and M.R. Poellot, Chemical characteristics of ice residual nuclei in anvil cirrus clouds:evidence for homogeneous and heterogeneous ice formation, *Atmos. Chem. Phys.*, 5, 2289–2297, 2005.

- Twomey, S.A., The influence of pollution on the shortwave albedo of clouds, *J. Atmos. Sci.*, *34*, 1149–1152, 1977.
- Usher, C.R., A.E. Michel, and V.H. Grassian, Reactions on mineral dust, *Chem. Rev.*, *103* (12), 4883–4939, 2003.
- Vali, G., Nucleation Terminology, *Bull. Amer. Meteorol. Soc.*, *66* (11), 1426–1427, 1985.
- Vali, G., Ice nucleation - a review, in *Nucleation in Atmospheric Aerosols*, edited by M. Kulmala, and P. Wagner, pp. 271–279, Pergamon Press, 1996.
- Wayne, R.P., *Chemistry of Atmospheres*, Oxford University Press, Oxford, 2000.
- Wijnja, H., and C.P. Schulthess, Vibrational spectroscopy study of selenate and sulfate adsorption mechanisms on Fe and Al (hydr)oxide surfaces, *J. Colloid Interface Sci.*, *229*, 286–297, 2000.
- Zhang, G.Y., and D. Peak, Studies of Cd(II)-sulfate interactions at the goethite-water interface by ATR-FTIR spectroscopy, *Geochim. Cosmochim. Acta*, *71* (2158–2169), 2007.
- Zhou, Z., and W.D. Gunter, The nature of the surface charge on kaolinite, *Clays and Clay Miner.*, *40* (3), 365–368, 1992.
- Zimmermann, F., M. Ebert, A. Worringer, L. Schütz, and S. Weinbruch, Environmental scanning electron microscopy (ESEM) as a new technique to determine the ice nucleation capability of individual atmospheric aerosol particles, *Atmos. Env.*, *41*, 8219–8227, 2007.
- Zuberi, B., A.K. Bertram, C.A. Cassa, L.T. Molina, and M.J. Molina, Heterogeneous nucleation of ice in $(\text{NH}_4)_2\text{SO}_4\text{-H}_2\text{O}$ particles with mineral dust immersions, *Geophys. Res. Lett.*, *29* (10), 1504, 2002.